Compositional range and crystal fractionation of basaltic pillows from Ármannsfell, SW-Iceland

Sigríður Inga Svavarsdóttir

Faculty of Earth Sciences
University of Iceland
2014

Compositional range and crystal fractionation of basaltic pillows from Ármannsfell, SW-Iceland

Sigríður Inga Svavarsdóttir

10 ECTS thesis submitted in partial fulfilment of
Baccalaureus Scientiarum degree in Geology

Advisor
Karl Grönvold

Faculty of Earth Sciences
School of Engineering and Natural Sciences
University of Iceland
Reykjavik, May 2014

Compositional range and crystal fractionation of basaltic pillows from Armannsfell, SW-Iceland
Compositional range of basaltic pillows
10 ECTS thesis submitted in partial fulfilment of a *Baccalaureus Scientiarum* degree in Geology

Faculty of Earth Sciences
School of Engineering and Natural Sciences
University of Iceland
Askja, Sturlugata 7
107 Reykjavík

Telephone: 525 4000

Registration information:
Sigríður Inga Svavardóttir, 2014, *Compositional range and crystal fractionation of basaltic pillos from Armannsfell, SW-Iceland*, Bachelor's thesis, Faculty of Earth Sciences, University of Iceland.

Printing: Háskólaprent
Reykjavik, Iceland, May 2014

Abstract

Olivine tholeiite pillows from Armannsfell, SW-Iceland, were collected in order to reveal chemical and mineralogical fractionation among the different lithofacies of the pillows; the rim, crust and core.

Whole rock composition of pillow units range from 11 to 20 Wt % ol in the norm. Detailed EDS analysis of rim-glass and residual glass shows dominating ol-tholeitie composition ranging from 15 % ol in the norm towards subordinate qz-tholeiite with 2.7 % qz in the norm. Minor intermediate and silicic residual glass is found in the pillow cores, ranging up to 25 % qz in the norm.

Detailed SEM and EDS analyses of the pillow units show that olivine phenocrysts (85 % Fo) and plagioclase (88 % An) microphenocryst in the pillow rim existed in a cotectic relation prior to eruption of the pillow basalt. The crystallization of ol (85-72 % Fo) and plag (88-64 % An) continues into the pillow crust where clinopyroxene augite enters the assemblage. Clinopyroxene with Ti-augite (5 Wt % TiO_2) composition is formed until titanomagnetite enters the mineral assemblage. Towards the end of crystallization, common augite (2 Wt % TiO_2) crystallizes with olivine, plagioclase and magnetite. Magnetite composition ranges from 70-59 % Usp in the absence of ilmenite.

Crystal fractionation of the melt and mechanical fractionation of ol phenochrysts along the pillows obscures the composition of the primary magma. This demands whole rock analyses of several pillow-units in order to find a representative sample of pillow basalt.

Útdráttur

Sýnum af ólivín-þóleiíti í bólstrabergi úr Ármannsfelli var safnað til að kanna efnafræðilegan og steindafræðilegan breytileika í mismunandi berggerðum bólstranna; glerrima, skorpu og kjarna.

Bergsamsetning bólstraeininganna er breytileg frá 11 í 20 % ol í normi. Ítarleg EDS greining á bólstragleri og afgangsgleri sýnir ríkjandi ol-þóleiít samsetningu þróast frá 15 % ol í normi í átt að smáræði af qz-þóleiíti með 2.7 % qz í normi. Í kjarna bólstranna finnst smáræði af ísúru og súru gleri allt að 25 % qz í normi.

Ítarlegar SEM og EDS greiningar sýna að ólivín (85 % Fo) dílar og plagíóklas (88 % An) míkrodílar voru í tvífasa jafnvægi fyrir gos. Olivín (85-72 % Fo) og plagíóklas (88-64 % An) halda áfram að kristallast inn í bólstraskorpuna þar sem ágít-klónópýroxen tekur að myndast. Ti-ágít (5 Wt % TiO_2) myndast þar til títanmagnetít fellur út. Við lok kristöllunar myndsat venjulegt ágít (2 Wt % TiO_2), ásamt ólivín, plagíóklas og títanmagnetíti. Magnetítsamsetningin er 70-59 % ulvöspínill en ilmenít myndast ekki.

Kristaldiffrun bráðarinnar og flæðidiffrun ólivín – og plagíóklas díla út eftir bólstrunum raskar samsetningu frumkvikunnar. Þetta krefst bergefnagreininga á allnokkrum bólstraeiningum til að finna dæmigert sýni af bólstrabergi.

Table of Contents

List of Figures

List of Tables

Abbreviations

MORB - Mid Ocean Ridge Basalt

WRZ- Western Rift-Zone.

SEM - Secondary Electron Microscopy.

Cp – Heat capacity

Wt% - Weight percentage

ICP - OES - Inductively coupled Plasma Optical Emission Spectroscopy.

EDS - Energy Dispersive Spectroscopy.

CIPW MORM - Cross, Iddings, Pirsson, Washington, NORM.

#Mg – Magnesium number, MgO/(MgO+FeO)

HFSE elements – High Field Strength elements.

LIL elements - Large Ion Lithophile elements.

%Mol – Molecular percentage

FMQ – Fayalite Magnetite Quartz.

R-NES – Reykjanes Peninsula.

BSE – Back Scattered Electrons

En – Enstatite.

Fs – Ferrosilite.

Wo – Wollastonite.

An – Anorthite.

Cpx – Clinopyroxene.

Acknowledgements

I wish to thank my supervisor, Dr. Karl Grönvold, for professional guidance and Niels Oskarsson for assistance in the lab.

My beloved are once again thanked for being there.

1 Introduction

Iceland is a subareal part of the North Atlantic rift system and is dominated by MORB-like olivine tholeiites that are the prominent basalt type of oceanic rifts. The rift relocations, along with Icelands underlying mantle plume cause the detailed chemistry to have a large range. The basaltic rocks extand from being primitive, based on high MgO and Mg/Fe, to being more evolved, displaying different degrees of partial melting (Oskarsson et al., 1982).

The most common view is that the most primitive MORBs have composition close to the primitive magma that it was derived from, implying insignificant crystal fractionation (Presnall and Hoover, 1984). O'Hara (1965) challenged this view by arguing that the chemical composition of basaltic rocks suggest that the magmas are generally residual liquids of a well advanced crystal fractionation process. If this is true, then the magmas have undergone a great deal of crystal fractionation during their ascent. Basaltic pillows dominate among fresh rock samples dredged from the ocean floors worldwide. Analysis of pillow basalts have contributed a great deal to the definition of MORB. It is, therefore, of some importance to evaluate the fractionation effect from a pillow formation in terms of simultaneous crystal fractionation and flow fractionation of minerals.

The object of the present study is to examine the magnitude of magma and mineral fractionation within basaltic pillows. Iceland is an ideal place for this kind of study because many volcanoes in Iceland were emplaced in sub glacial conditions during the last glacial period. The method chosen was to sample a number of pillows, their rims, crusts and interiors from a radial cut cross section through an almost perfect pillow outcrop at the base of the subglacial hyaloclastite mountain Armannsfell (Figure 1). The pillows were chosen by their amount of glass at their rims, but as Figure 1 shows they were different in size and shape. Glass samples from pillow rims are very important chemically because they can represent the liquid compositions at the time of cooling. The basic premise of the method is that a reasonably high number of pillow samples from the rim, crust and interior will reveal all the compositional variation there is within the section. Description of the samples taken from the outcrop are listed in Table 1.

Table 1. Description of the samples taken from the pillow basalt outcrop in Armannsfell.

Sample	Pillow nr.	Description of sample
G1	1	Glass sample from the pillow rim
M1	1	Rock sample from the pillow crust
K1	1	Rock sample from the pillow core
G2	2	Glass sample from the pillow rim
G3	3	Glass sample from the pillow rim
G4	4	Glass sample from the pillow rim
M4	4	Rock sample from the pillow crust
K4	4	Rock sample from the pillow core
G5	5	Glass sample from the pillow rim

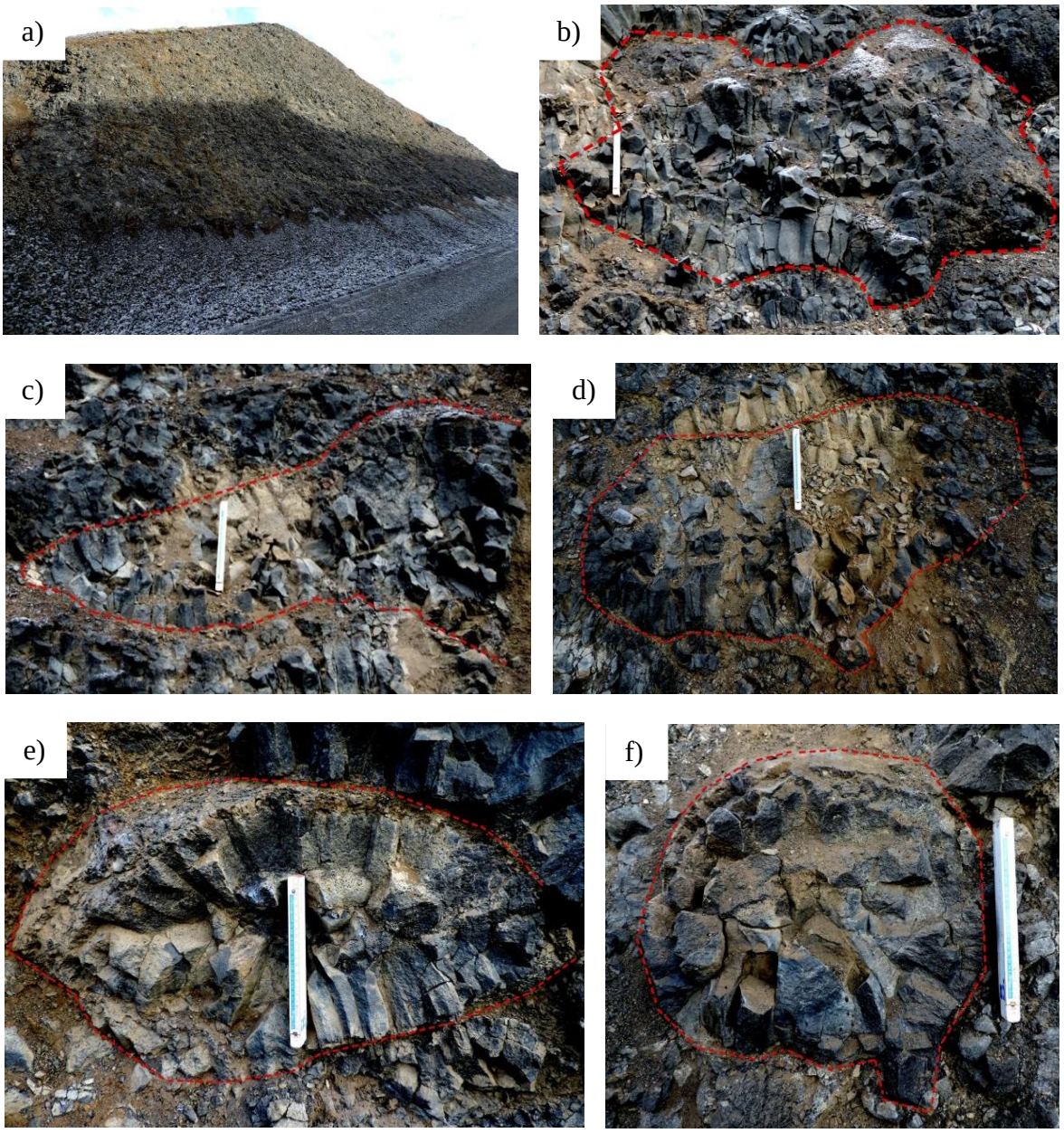

Figure 1. The pillow basalt outcrop and individual pillows. a) The outcrop at the base of Armannsfell (64°19'34 N, 20°59'53 W). Figure b) to f) are of individual pillows, marking b) for pillow No. 1, c) for pillow No. 2, and so on.

Sinton, Grönvold & Saemundarson (2005), identified 34 separate post glacial eruptive units in the Mid-Western Rift-Zone (WRZ) of Iceland, in addition to 10 small units that comprise the Grímsnes field. A basic part of the study was the detailed chemical analysis that revealed the divisions of some mapped units into two or more separate eruptive sequence, each with a distinctive range of chemical composition. Also, they divided the postglacial eruptive history of the WRZ into four general age subdivisions, with Armannsfell as a part of eruptions from Pleistocene. Sinton (2009) modified a geological map of the WRZ, showing post-glacial lava units, Fini-glacial lava units and Pleistocene

units. Figure 2 shows an enlargement of the geological map, with an arrow pointing to the research area.

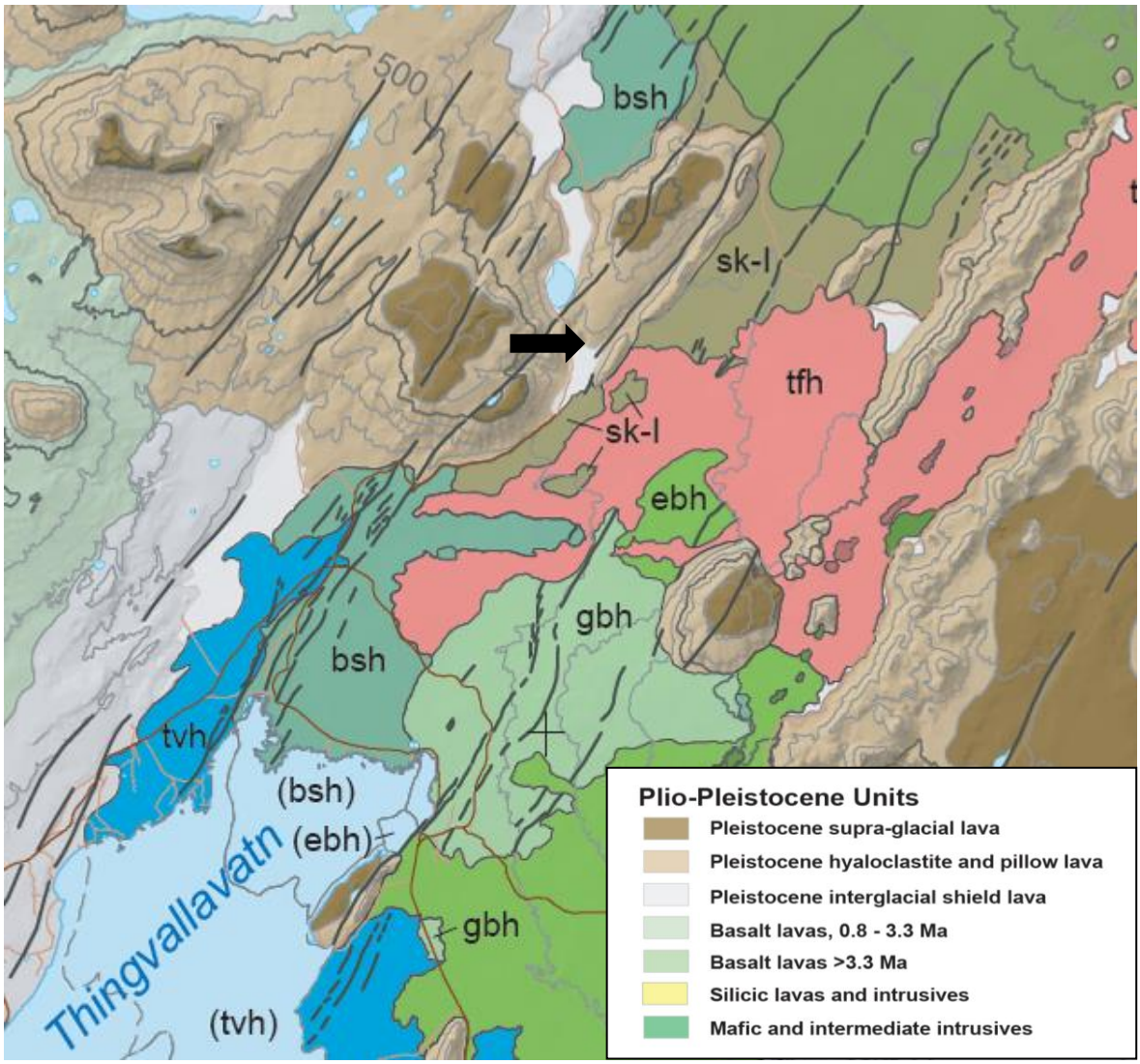

Figure 2. Geological map showing the middle part of the WRZ. The black arrow points to the pillow basalt outcrop at the base of Armannsfell, where samples were collected from. (Adapted from Sinton, 2009).

1.1 Pillow formation and their sampling

Pillows form where the water pressure is high enough to prevent efficient mixing of magma and water that otherwise leads to phreatomagmatic eruptions. Therefore, pillow lavas make up the basal unit of hyaloclastite formations in tuya-mountains and hyaloclastite ridges. In the WRZ, elongated ridges of pillow lava are commonly observed, which may have formed when basaltic lava flow entered glacial melt-water in subglacial drainage channels (Jakobsson and Gudmundsson, 2008).

Pillow basalts form elongated lava-tubes that are usually 0.5-1.0 m in diameter (Jakobsson and Gudmundsson, 2008). Their size and shape variations are primarily controlled by viscosity of the magma and the eruption rate. Hoskuldsson (2013) divided the cooling history of a pillow pile into two stages; the first stage being cooling of the pillow as it erupted into the standing water, and the second stage cooling of the pillow as it's buried under the pillow pile. After the pillows get buried, steam intruding throughout the pillow pile controls the cooling of individual pillows and the cooling rate slows down (Hoskuldsson, 2013).

The rapidly quenched glassy rims of pillows are thus, the only part of the pillow controlled by the first stage of cooling. Soon, a cryptocrystalline crust of rock forms and partially isolates the flowing interior from the external cooling medium. Axial flow of magma within the pillow supplies thickening of the crust from inside while gas bubbles form at the interface due to crystallization of the anhydrous rock forming minerals. Since crystallization on the inside of the crust separates minerals from the flowing magma the solidification process resembles forced crystal fractionation that results in chemical evolution of the moving liquid.

In theory, the snout of an advancing pillow is formed by successively more evolved melt as compared with the pillow root. Since the inflow of melt has a constant initial composition it follows that the interior of a pillow also may have compositional gradation along its length. Degassing of juvenile water from the liquid will inevitably increase its viscosity by increased polymerization of silica leading to rapid growth of the rock forming minerals. The inevitable increased flow-resistance within the pillow tube may lead to rupture of the pillow crust and the formation of a new pillow lobe. This scenario involves prolonged flow of unfractionated primary magma within the root (inlet) of the pillow. After solidification, the crystalline conduit forms the pillow core.

The petrological consequences of the pillow formation process is the main theme of the present study. It is by no means clear what a single sample of a pillow rim, crust or core means in terms of initial magmatic composition. The basic premise of this study is to analyse the lithological units of few pillows from the Armannsfell outcrop in order to define the magnitude of the fractionation processes at work during their formation. This is achived by sampling of all the lithofacies of several pillows and their detailed mineralogical and chemical analysis.

2 Formation and petrography of basalt pillows

Lithofacies of pillow basalt, indicated in Figure 3 and Figure 4, fall into three different groups that reflect different cooling rates;

a) The pillow rim is composed of volcanic glass that also contains the phenocrysts and xenocrysts that may have existed in the magma during eruption. Microlites of liquidus minerals generally start to form within the rim. Thickness of pillow glass rims is slightly variable on the scale of 1-3 cm. Pillow glass samples in the tables are labelled with G.

b) The pillow crust is a cryptocrystalline to very fine grained rock that solidifies at high rate from the crust-rim interface towards the core. Low amount of volcanic glass can occasionally be found within the outer rim but generally the crust is a holocrystalline mass with small bubbles that form during crystallization as gases are expelled from the magma. In a typical pillow outcrop, the crust is fractured into wedges by radial cooling cracks. Cracks in the cooling crust (Muller, 1998) may be assumed to form at temperatures between 600°C and 900 °C when the contraction rate is at its maximum (yield region). These fractures will inevitably favour the ingress of supercritical steam into the cooling and crystallizing magma. Occasionally, steam-oxidized fractures are found within pillow crusts. Pillow crust samples are labelled with M.

c) The pillow core is a medium to coarse grained basalt with abundant vesicles, commonly enriched within the upper section of the core. Irregular cooling cracks may split the core into bolder sized vesicular blocks. Pillow core samples are labelled with K.

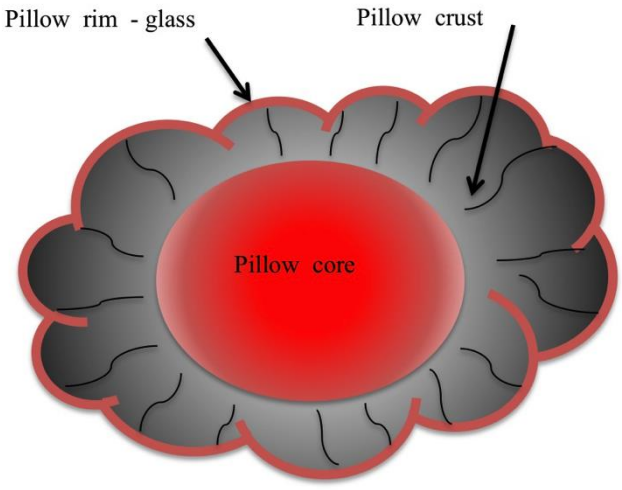

Figure 3. The Figure shows a schematic cross section through a basalt pillow. The orange line indicates the pillow rim that is a small part of the total mass while the pillow crust and the pillow core are variable in thickness depending on cooling time. Cooling cracks indicated in the Figure form as the crust thickens and cools below temperature of about 900 °C.

Basaltic pillows that form at pressures low enough to permit degassing of the magma are characterized by accumulation of gas bubbles or even gas filled channels below the roof of the core as well as accumulation of phenocrysts along the bottom layer. Even if primary degassing of the magma is absent either due to high confining pressure or low volatile content of the magma, gas bubbles will inevitably form during the latest stages of crystallization. This is the consequence of enrichment in volatiles in the intergranular residual melt during growth of the anhydrous rock forming minerals. Pillow-cores most commonly show sub-ophitic to ophitic textures that resemble textures of basaltic lava flows.

There is a marked difference among basalt pillows regarding the relative thickness of the crust and the core. Figure 4 outlines the variable thickness of the crust and the core diameter along a pillow. Cooling time is longest at the root where also the crust reaches its maximum thickness. Minimum core diameter is also found at the root that serves as magma inlet during lengthening of the pillow-tube. It is obvious that the closure of the inlet by thickening of the crust is the process that terminates the inflow into the pillow tube.

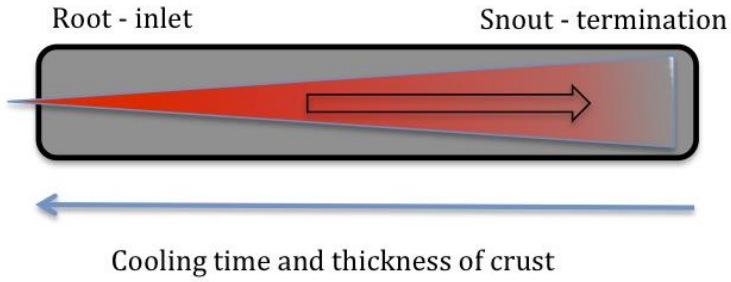

Figure 4. The Figure shows schematic length section along basaltic pillow. The pillow length is variable, mostly in the order of 5-7 m. In the Figure the thin black outer line of the pillow reprecents the rim, the gray area reprecents the crust, while the orange area reprecents the core.

In Figure 1, pillows from the Armannsfell outcrop show the different thickness of crust and core very clearly. Figure 1f shows a section through the termination of a pillow, the thin crust is just a band inside the rim while the core makes up most of the section. In Figure 1b a moderately thick crust and core indicate section through the middle part of a pillow pipe. In Figure 1e the core is very small, indicating section close to the root.

Formation of a basalt pillow involves some material fractionation; the pillow rim which forms at the snout is made of material that has lost considerable mass to the pillow crust along the tube. Similarly, the core at the snout has lost material to the crust along the entire length of the pillow. Accordingly, the core at the root is made up of the last and least fractionated magma that entered the pillow tube.

When basaltic melt cools it loses energy to the surroundings, and it forms crystals in the order of decreasing entropy (Winter, 2010). In olivine tholeiite at low pressure this order is olivine, plagioclase, pyroxene and the last crystals to form are oxides. The crystallization sequence in pillow basalts forms at extremely fast rate during quenching of the glass and formation of the pillow crust, but at slightly slower rate within the pillow interior that

eventually forms the pillow core. Petrography and crystallization order of rocks can be analysed quite well using SEM-BSE images.

Figure 5 shows a section through the outer rim of the pillow in sample G4, Table 1. Despite of fast cooling, the pillow glass contains olivine phenocrysts and oxide microphenocrysts, which must be crystals that were already in the magma before it reached the surface.

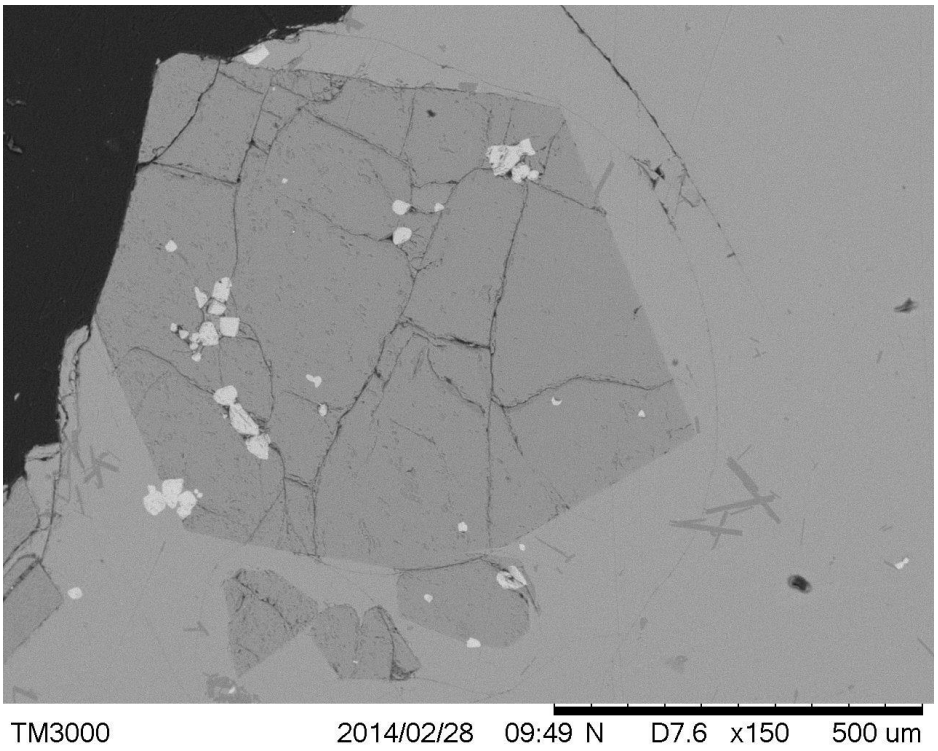

Figure 5. SEM image of sample from the rim of pillow No. 4 (G4, Table 1.). In the middle of the Figure is a big olivine phenocryst with oxide inclusions, and small plagioclase list in the glass around the crystal.

The olivine phenocryst in the middle of Figure 5 is about 600 µm in diameter, and contains inclusions of oxides, presumably chromite. Euhedral olivine is common as phenocryst in basalt (Gribble and Hall, 1992). The Figure also shows that small plagioclase lists (50-100 µm) have formed in the glass.

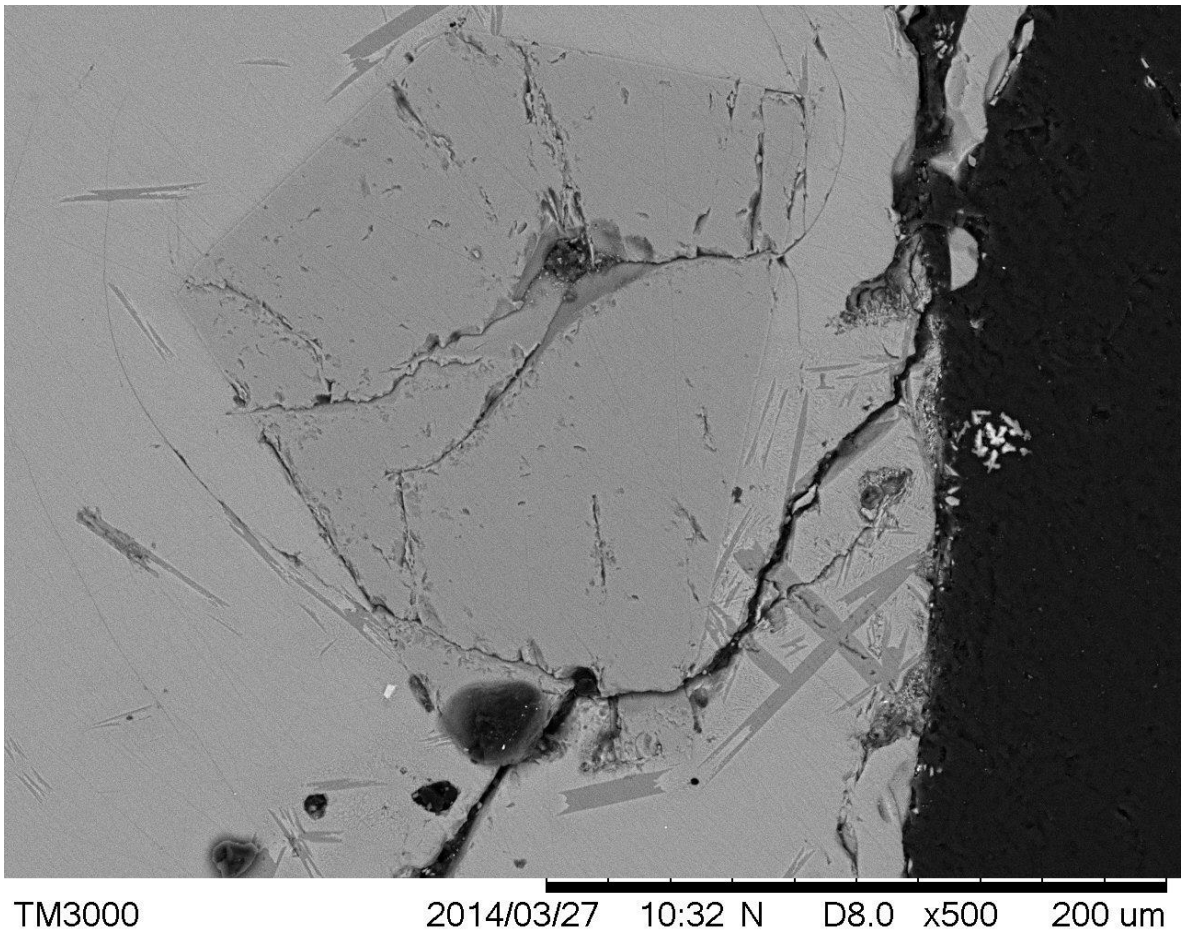

Figure 6. SEM image of sample from the rim of pillow No. 4 (G4, Table 1.). The Figure shows a large olivine phenocryst in the center that is surrounded by small plagioclase lists in the glass.

Figure 6, also shows a section through the outer rim of the pillow glass in sample G4. The olivine phenocryst in the center of the Figure is about 200 µm in diameter, surrounded by small (50-100 µm) plagioclase lists. This olivine crystal shows no signs of Fe-Mg zoning and no signs of dissolution precipitation reaction at the margins, which reflects a perfect equilibrium with the melt. Note the alignment of plagioclase lists, larger than the average, around the edges of the olivine crystal in the upper middle and on the base of the Figure. When this area is closely examined, the evolving texture seems to be different from the aphyric glass and small gas bubbles are forming (Figure 6, lower middle) among the crystals. The glass between the plagioclase lists and the olivine phenocryst is evolving into cryptocrystalline domains. Therefore, we might be seeing the beginning liquid polymerization into clinopyroxene. This is, indeed, expected where the gas, presumably water vapor, had the time to reach saturation state followed by degassing that increases the liquidus temperature but the cooling was too fast for the actual crystallization to start.

In Figure 6 the plagioclase lists, significantly larger than average, that surround the olivine phenocryst may be explained by slower cooling of the melt around the crystal. At temperatures between 1100°C and 1200°C the heat capacitiy (Bouhifd et al., 2007) of olivine (Cp_{ol} =1.15 J/gK) is significantly higher than that of basaltic glass (Cp_{gl} = 1.05 J/gK) which results in slower cooling of the olivine and the glass layer surrounding the

phenocryst. This slower cooling around the olivine seems to give time enough for the plagioclase to reach length of some 100 µm.

Growth rate, expressed as growth of the fastest-growing crystal plane, of plagioclase in basaltic magma certainly depends on the cooling rate and undecooling but also on the water saturation of the melt. Orlando et al. (2008) determined maximum growth rate of 10^{-5} mm/min for plagioclase in anhydrous trachybasaltic melt at temperatures 1160-1240 °C at 20 °C undercooling. Munchill and Lasaga (1987) determined growth rates of $5x10^{-1}$ mm/min in anhydrous plagioclase melt at 1 atm pressure. This experimental difference in growth rate of four orders of magnitude suggests that estimated plagioclase growth as a function of cooling rate in basalts, as worked out by Cashman (1993), may be the most realistic scenario for a basaltic pillow rim. The highest cooling rate corresponds to growth rate of $21.5x10^{-1}$ mm/min or 150 µm/min which implies that the largest (100 µm) plagioclase in Figure 6 grew during some 40 seconds.

Since the growth rate of a crystal slows markedly at lower cooling rates the crystal size will not increase linearly with distance from the rim. On the contrary, we might expect abundant very small crystals throughout the entire pillow.

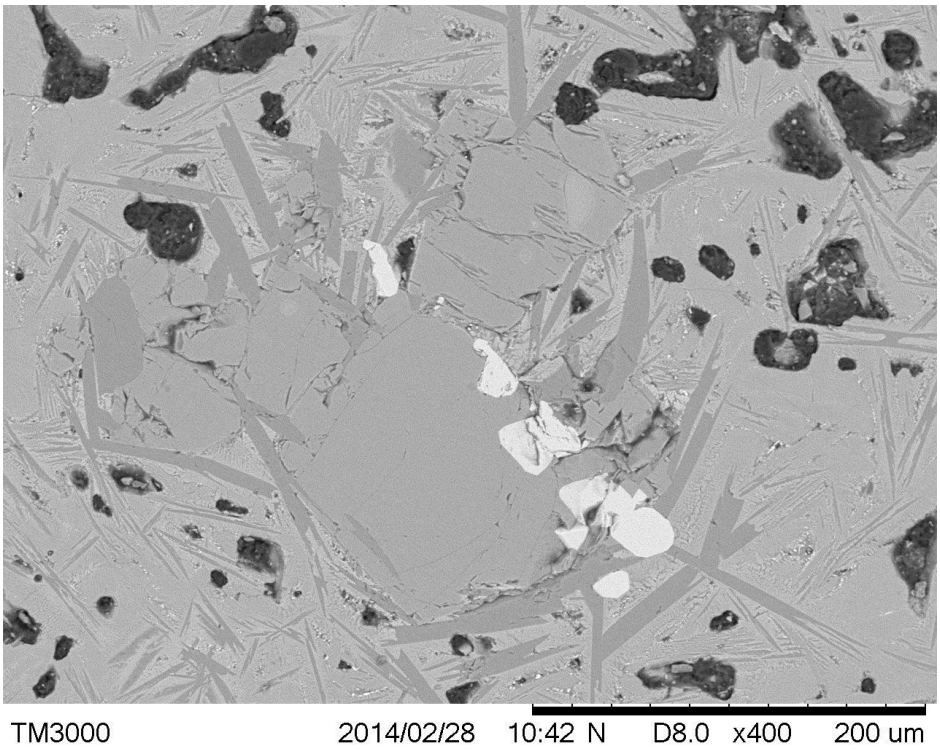

Figure 7. SEM image of glass sample from the rim of pillow No. 4 (G4). The Figure shows the inferred stage of crystallization after the scenario of Figure 6. Here the plagioclase lists are larger and gas bubbles are more abundant.

Figure 7 shows olivine crystal with inclusions of chromite in pillow rim sample G4 surrounded by 100–150 µm long plagioclase lists and gas bubbles. Here, the process outlined in Figure 6 is shown at a more advanced state; larger plagioclase lists surround the olivine and numerous small plagioclase lists have nucleated in the melt. An estimated time interval between the scenarios in Figure 6 and Figure 7 is in the order of 10 seconds

assuming the growth rate 150 mm/min. An additional feature shown by Figure 7 is the high abundance of gas bubbles. Most of the bubbles are well rounded but some are shaped by the adjoining crystals. In the upper middle of the figure the glassy mass between crystals shows the onset of clinopyroxene growth.

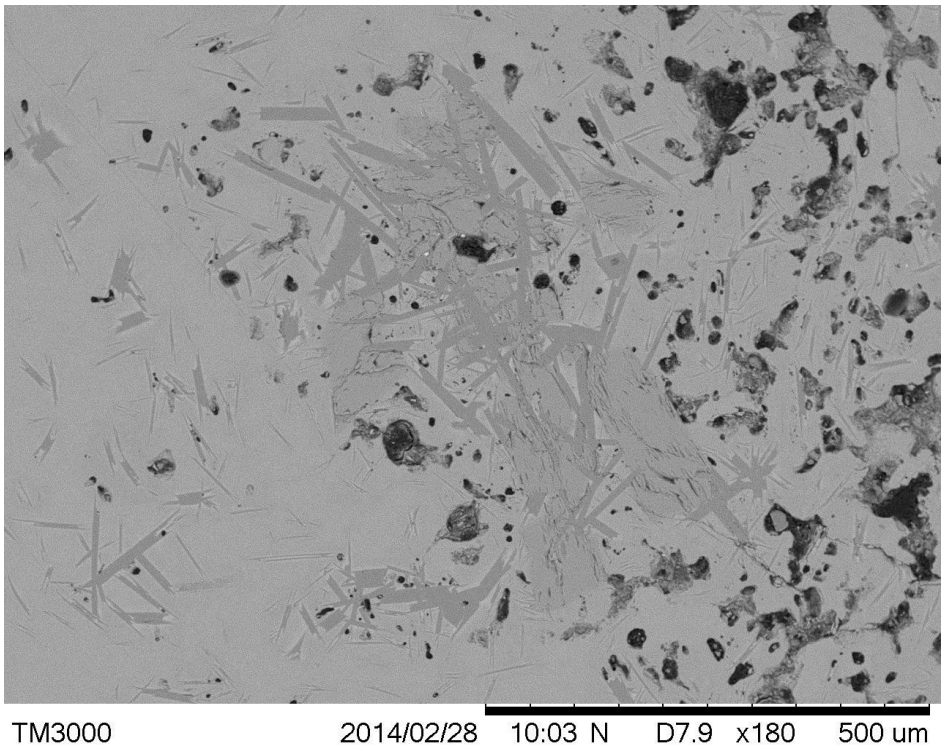

Figure 8. SEM image of glass sample from the rim of pillow No. 4 (G4). The Figure shows the margin of glass and crystalized groundmass in the sample, this is the domain where gas bubbles become much more abundant.

The margin between pillow rim glass and crystalized pillow core groundmass can be seen in Figure 8. It is clear that close to the pillow interior, gas bubbles become more abundant. This happens because of the pervasive crystallization of the pillow crust. The magma crystallises to a point where it forms a rigid crystal framework, and volatiles escape from the residual liquid (Rogan, Blake and Smith, 1996). Formation of the pillow crust will, on the other hand prevent the escape of gas from the flowing interior that forms new rim and crust along the pillow and eventually the pillow core.

The volume fraction of gas bubbles that can be estimated from sections of totally degassed rock at the rim-crust boundary (Figure 8) amounts to at least 25% gas volume. This bubble volume may be taken as an indication of the amount of dissolved gas before extrusion of the pillow. This may also be a criterion for the water content of the magma, assuming that the bubbles were filled with steam. Assuming also ideal gas behaviour at liquidus temperature of 1200°C and pressure of 100 atm, corresponding to about 1 km ice cover, the calculated water content is only 0.18 Wt % H_2O.

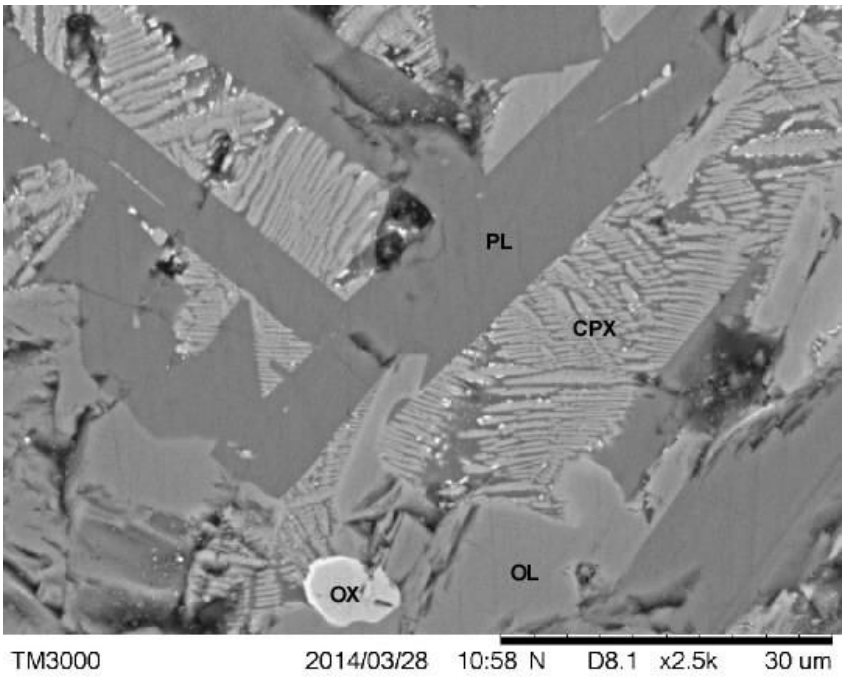

Figure 9. SEM image of rock sample from the crust of pillow No. 1 (M1, Table 1). The Figure shows the formation of clinopyroxene and oxides between the pre-existing plagioclase lists and olivine. The intergranular Ti-augite forms in feathers and dendritic until titanomagnetite (bright spots) becomes stable. Subsequently formed clinopyrocene is common augite.

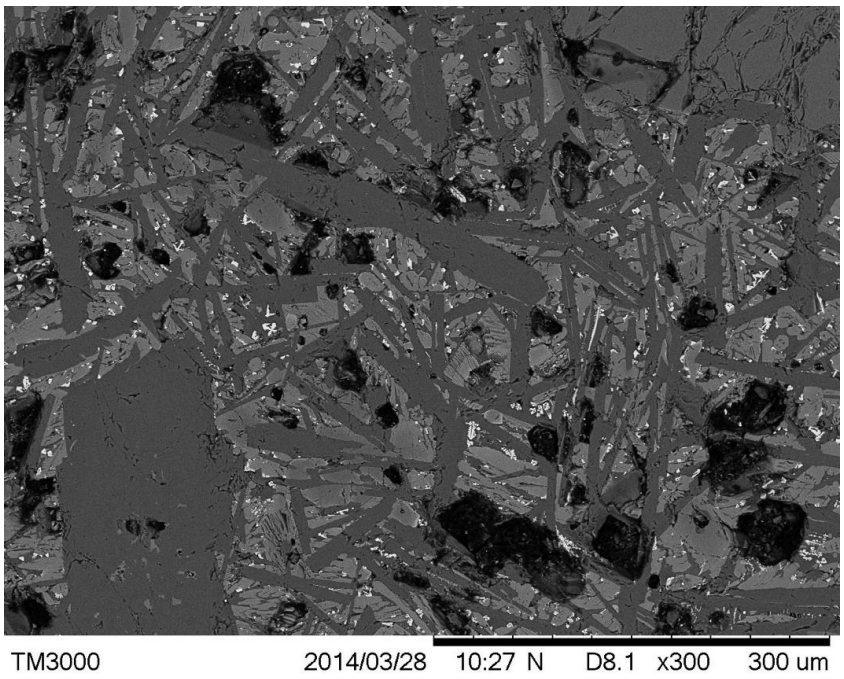

Figure 10. SEM image of rock sample from the core of pillow No. 1 (K1). The Figure shows fully crystallized groundmass of pillow core, where "large" plagioclase lists are separated by clinopyroxene. Minute titanomagnetite grains are set in the clinopyroxen matrix on the junction between Ti-augite and augite. Phenocrysts of plagioclase in the lower left and olivine in the upper right are seen in the otherwise supophitic texture.

An almost complete crystallization of the liquid in sample M1 (Table 1) can be seen in Figure 9. Skeletal crystals of clinopyroxene are filling up the spaces between these pre-existing phases, which are plagioclase and olivine. Single chromite phenocryst is also in the groundmass, resembling the chromite that were found in the glass rims. Small nuclei of titanomagnetite appear as small white dots outside the skeletal clinopyroxenes.

Figure 10 shows the almost fully crystalized interior of sample K1, Table 1. Many of the plagioclase lists are 200-300 micrometres in length, so it is clear that the lists grow in size closer to the core, with increasing crystallization. At this stage all phases except the Ti-augite exist in equilibrium and are filling up the gaps between the large plagioclase lists.

Note the “large” plagioclase in the lower left and the plagioclase list, about 230 µm long, in the upper middle of the Figure. Olivine occurs as small equant grains while the clinopyroxene fills the interstitial space. Apart from crystal size, the difference in the core texture and the crust texture is that in the core the clinopyroxene are common augite and the titanomagnetite has evolved into euhedral dendritic microliths.

Summarizing the petrographic results reveals three epochs of crystalization:

a) Pillow rim: Pervasive nucleation of plagioclase and degassing of the melt due to crystallization occurs rapidly at the rim-crust boundary.

b) Pillow crust: Continued growth of olivine phenochrysts and plagioclase microphenocrysts followed by nucleation of intersititał clinopyroxen augite, sometimes titanaugite, and titanomagnetite microliths.

c) Pillow core: Growth of all minerals into subophitoc texture resembling “ordinary” basaltic lava.

Also inferred from the petrographic analysis of plagioclase is that the pillow rim formed on the time scale of seconds to minutes and the crust on the time scale of minutes. Based on volume estimate of gas bubbles it is inferred that the magma contained no more than about 0.2 Wt % H_2O.

3 Analytical results: Compositional range of rocks, glass and minerals

Whole rock chemical analyses done by ICP-OES (Appendix A), reflect compositional differences within the pillow that are due to crystal fractionation during flow and mechanical fractionation of minerals. Composition of glass is important because it is the the most sensitive indicator of liquid composition at the time of quenching. Detailed EDS microbeam analyses were made on rim section from pillows No. 2 and No. 4 to record the glass composition from the pillow surface towards the pillow crust. Mineral compositions were also recorded by EDS analyses for quantifying compositional changes from the pillow rim towards the core.

3.1 Whole rock composition

Glassy rims of 5 different pillows were separated for whole rock chemical analyses by ICP-OES (Appendix A). Two pillows, No. 1 and No. 4 were further separated into two samples of cryptocrystalline pillow-crusts, about 2-3 cm from the pillow-margin and two samples of medium to fine grained samples from pillow-cores. The oxidation state of iron in all samples was also measured by titration of FeO (Appendix C) according to the Wilson method (Wilson, 1955). Chemical composition and CIPW-norm of these samples are listed in Table 2. The rocks are typical olivine tholeiite with abundant hypersthene (6-15 Wt%) in the norm and normative olivine ranging from 11-20 Wt%, slightly depending upon the oxidation state of iron.

Table 2. Chemical analysis (Wt %) and CIPW (Wt %) norm of samples derived from the pillow basalt outcrop at the base of Armannsfell.

Sample:	G1	M1	K1	G2	G3	G4	M4	K4	G5
SiO_2	46.43	44.21	46.43	45.66	47.74	46.45	46.33	46.15	46.82
TiO_2	1.97	1.91	1.90	1.80	1.94	1.98	1.95	2.00	1.91
Al_2O_3	14.48	14.29	14.28	13.65	14.29	14.43	14.73	14.85	14.11
Fe_2O_3	2.15	1.08	1.61	1.55	2.44	1.46	1.65	1.32	2.09
FeO	9.88	10.54	10.41	10.54	10.05	10.63	10.10	10.30	9.94
MnO	0.21	0.20	0.20	0.21	0.21	0.20	0.20	0.20	0.20
MgO	9.09	8.70	9.68	11.98	10.76	9.35	8.62	7.87	9.81
CaO	10.61	10.83	10.90	9.91	10.74	10.92	11.10	11.46	10.72
Na_2O	1.89	1.93	1.89	1.76	1.93	1.99	2.11	2.00	1.85
K_2O	0.15	0.17	0.15	0.14	0.15	0.15	0.16	0.16	0.15
P_2O_5	0.16	0.16	0.16	0.16	0.17	0.17	0.17	0.21	0.16
FeO-TOT	11.82	11.51	11.86	11.94	12.25	11.95	11.59	11.49	11.82
NORM									
Quartz	0.0	0.0	0.0	0.0	0.0	0.0	0.0	0.0	0.0
Plag	46.6	46.2	46.0	43.8	46.2	46.8	48.1	48.0	45.4
Diopside	17.2	18.8	18.8	15.6	18.2	18.9	19.5	20.1	18.3
Hyperst	15.5	6.5	12.1	11.8	13.7	10.9	9.1	11.0	15.3
Olivine	11.7	16.7	14.7	20.5	16.2	15.0	14.4	11.2	12.7
Ilmenite	3.7	3.6	3.6	3.4	3.7	3.8	3.7	3.8	3.6
Magnetite	1.0	0.9	1.0	1.0	1.0	1.0	0.9	0.9	1.0
Apatite	0.4	0.4	0.4	0.4	0.4	0.4	0.4	0.5	0.4
Ba	0.0052	0.0046	0.0047	0.0046	0.0051	0.0049	0.0047	0.0048	0.0049
Co	0.0068	0.0064	0.0067	0.0078	0.0074	0.0068	0.0064	0.0061	0.0069
Cr	0.0389	0.0401	0.0491	0.0573	0.0461	0.0387	0.0466	0.0300	0.0428
Cu	0.0163	0.0125	0.0132	0.0108	0.0140	0.0128	0.0145	0.0135	0.0139
Ni	0.0193	0.0166	0.0211	0.0308	0.0248	0.0199	0.0158	0.0170	0.0223
Sc	0.0039	0.0038	0.0037	0.0036	0.0039	0.0039	0.0038	0.0039	0.0038
Sr	0.0186	0.0181	0.0179	0.0171	0.0186	0.0187	0.0185	0.0192	0.0177
V	0.0307	0.0310	0.0305	0.0284	0.0303	0.0313	0.0317	0.0324	0.0306
Y	0.0031	0.0031	0.0030	0.0028	0.0030	0.0031	0.0030	0.0031	0.0030
Zn	0.0091	0.0090	0.0091	0.0091	0.0093	0.0091	0.0091	0.0089	0.0089
Zr	0.0098	0.0098	0.0095	0.0090	0.0097	0.0098	0.0100	0.0103	0.0097

There is no clear compositional difference among the three lithofacies although the pillow glass samples are slightly higher in MgO as compared with the cryptocrystalline pillow crust and the core basalt. An important tentative result is, however, that in both pillows No. 1 and No. 4 the surface glass is higher in MgO than the corresponding cryptocrystalline pillow cover. Composition of the pillow cores is, however, contrasting; core No. 1 is

higher in MgO than the rim samples and core No. 4 is lower in MgO. The core composition is tentatively assumed to be more affected by mechanical crystal cumulation and, accordingly, crystal loss when compared with the crust and the rim.

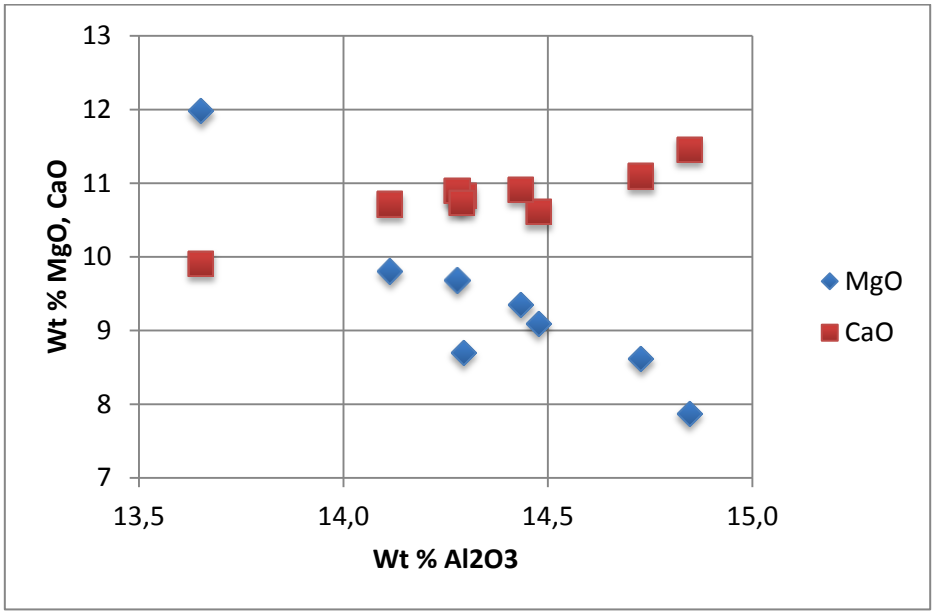

Figure 11. MgO, CaO and Al_2O_3 relations in whole rock fragments of 5 basalt pillows. In the Figure the red boxes show CaO-Al_2O_3 relations, while blue diamonds show MgO-Al_2O_3 relations.

Taken together, all the samples define a homogeneous chemical trend in major and trace elements. In Figure 11 the relations among MgO, CaO and Al_2O_3 show two trends that a positive correlation of Ca and Al but a negative correlation between Mg and Al. These trends indicate that the compositional difference among the samples is largely controlled by their plagioclase and olivine content.

A further indication of olivine control of MgO is found in the relations among MgO and Co, Cr and Ni which is enriched in the olivine due to the high partition coefficient Kd (Co=2, Cr=25, Ni=25) for Ni in olivine (Nielsen, 2014).

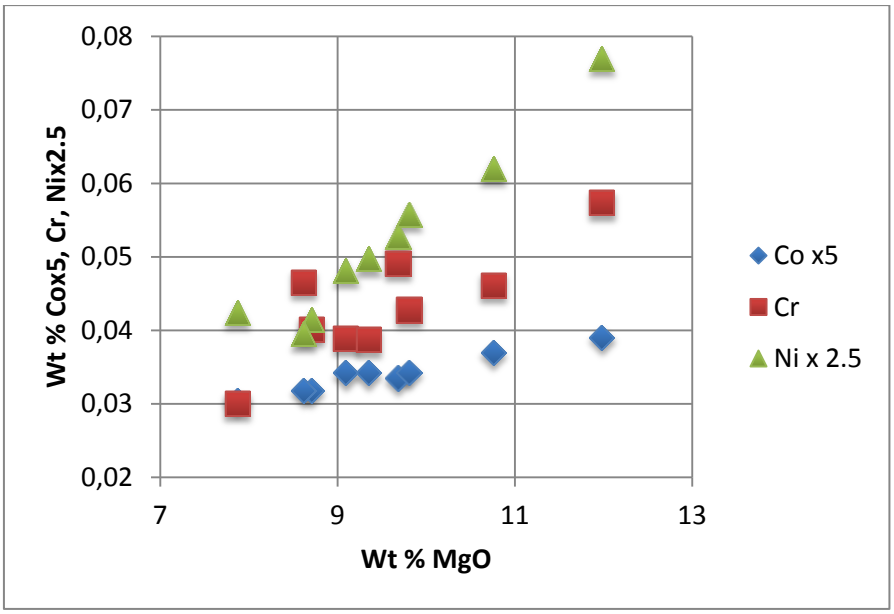

Figure 12. MgO-Co-Cr-Ni relations in basalt pillows. In the Figure green triangles show Mgo-Nix2.5 relations, red boxes show MgO-Cr relations, and blue dimonds show MgO-Cox5 relations.

In Figure 12, the positive correlation of the transition metals and MgO is obvious indicating a pervasive compositional control by olivine. However, the scatter in Cr also indicates the abundant chromite that occur both as microphenocrysts and inclusions in the olivine.

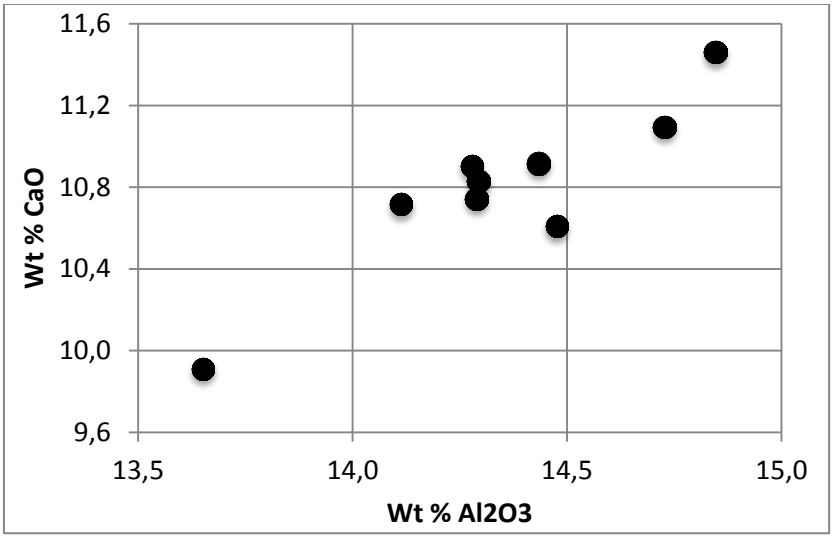

Figure 13. The Figure shows CaO-Al_2O_3 relations in basaltic pillows.

In Figure 13 the stong correlation suggests that these elements are controlled by the amount of plagioclase in the rock. In Table 2 the normative amount of plagioclase is about 46 Wt%. Normative composition of the rock also indicates different amount of diopside which also is a Ca mineral. It seems likely that Figure 13 displays different proportion of plagioclase and clinopyroxen in the rock.

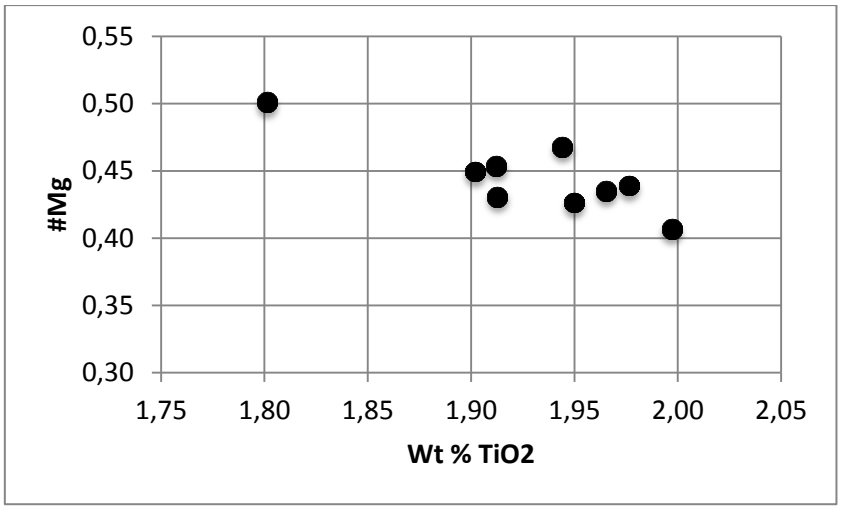

Figure 14. The Figure shows #Mg-TiO_2 relations in basaltic pillows.

In Figure 14, the #Mg that reflects the primitivity of the rock falls in proportion to TiO_2. This indicates that groundmass of the pillow basalt becomes enriched in HFSE and LIL elements as is also displayed in Table 2. In Figure 14 the sample in the upper left is glass from the pillow rim (sample G2 in Table 2) that contains abundant olivine phenocrysts. This sample contains about 1.8 Wt % TiO_2 but the main group contains between 1.9 and 2.0 Wt %. This indicates that if this difference is created by fractionation of crystals, the most magnesian samples my contain up to 10 Wt % more olivine than the average samples. Major element composition of the samples reflects almost perfectly the observations of the texture and mineral growth in the chapter on petrography.

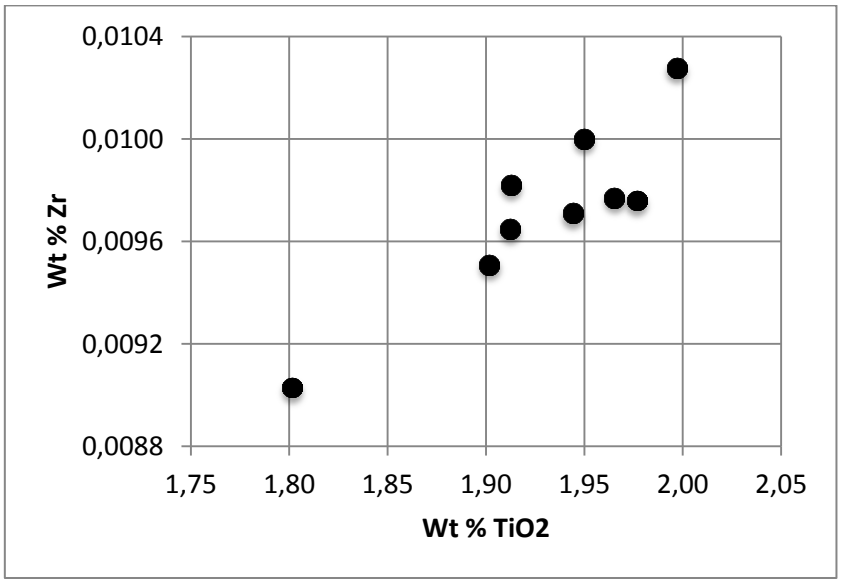

Figure 15. The Figure shows Zr-TiO_2 relation in basaltic pillows.

A perfect positive correlation would be expected for the two HFSE, Zr and Ti. In Figure 15 such correlation is definitely at hand but few of the Ti-rich samples deviate from the trend. It is obvious from the petrography section that formation of titanomagnetite towards the end of crystallization proceeded at different rates and in different quantities. There is a strong evidence that the formation of titanomagnetite depends on the oxidation state of the

silicate liquid. Therefore, an oxidized part of a pillow may precipitate titanomagnetite in such abundances that the mineral may be fractionated, creating a slight deviation from a linear Zr-TiO-TiO_2 trend as evident in Figure 15.

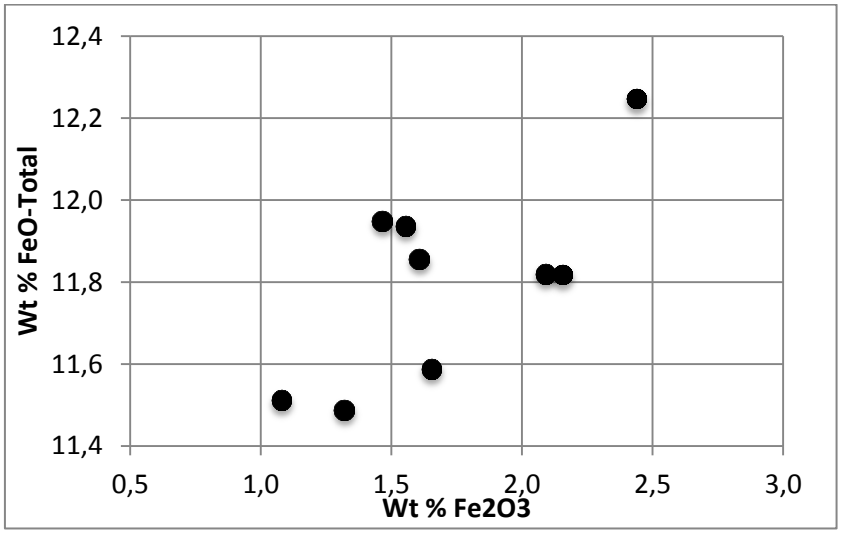

Figure 16. The Figure shows FeO total-Fe(III) relations in pillow basalt.

In the present rock suite the oxidation differences as derived from FeO analysis (Table 2) indicates different oxidation that may arise from mineral fractionation. In figure 16 the positive relation between total iron and Fe(III) suggests that crystallization of olivine and plagioclase both remove Fe(II) and increases the total iron content of the remaining melt. The side effect is that the increased Fe(III)/Fe(II) ratio of the melt favors titanomagnetite precipitation as is indeed, confirmed by the petrographic study.

3.2 Chemical composition of pillow glass

Glass rims from the pillows in Armansfell are thin, mostly below 1.5 cm in thickness. Rim section from two pillows, No. 2 and No. 4 were selected for detailed microbeam analysis by EDS (Appendix B) where the glass composition was recorded from the surface towards the cryptocrystalline pillow crust. Further glass analyses were made on the interstitial glass of the cryptocrystalline crust and within the cores of these pillows. The results of the Glass analysis are listed in Table 3.

The chemical analysis of the glass (Table 3) show interesting change in composition from olivine tholeite, towards qz-tholeiites and even dacitic composition in the most evolved samples. As seen in the averages for glass-rim samples No. 2 and No. 4 these samples are identical, on average. In Table 3, interstitial glass analyses from pillow core No. 4 (K4 3, K4 14, K4 29) and one crust sample (G4M39) show evolution trend towards intermediate and silicic composition, reaching dacitic composition in samples K4 3 and K4 14. Dacite is an acid volcanic rock with Si 63 Wt% or higher (Winter, 2010), which means that it is much more evolved than expected in the interior of basaltic pillow.

Table 3. Microbeam chemical analyses of glass from the basaltic pillow surface towards the cryptocrystalline pillow crust, arranged in order of decreasing MgO.

Pillow-rim glass sample analyses (G2)

Sample	SiO_2	TiO_2	Al_2O_3	FeO	MnO	MgO	CaO	Na_2O	K_2O	P_2O_5
G2 23	48.73	2.19	15.72	11.54	0.18	8.59	10.55	2.29	0.09	0.13
G2 3	48.33	2.04	15.56	11.99	0.10	8.58	10.72	2.34	0.10	0.25
G2 35	48.14	1.94	15.65	12.21	0.12	8.57	10.72	2.35	0.13	0.17
G2 8	49.38	2.07	14.09	13.05	0.16	8.25	10.86	1.89	0.09	0.15
G2 2	49.98	1.99	15.71	11.19	0.13	8.19	10.23	2.17	0.09	0.34
G2 33	47.04	2.54	14.71	12.88	0.15	8.14	11.52	2.22	0.22	0.58
G2 34	49.08	2.27	14.76	11.47	0.21	8.10	12.05	1.80	0.07	0.18
G2 4	49.11	2.04	15.05	11.89	0.14	8.02	11.74	1.77	0.07	0.18
G2 12	48.79	2.05	15.14	12.23	0.24	7.99	11.08	2.18	0.16	0.15
G2 19	48.66	2.23	15.33	11.80	0.20	7.88	11.50	2.10	0.17	0.13
G2 19	49.59	2.19	14.97	11.95	0.16	7.68	11.25	1.92	0.08	0.22
G2 28	49.12	2.30	14.77	12.24	0.17	7.65	11.50	1.91	0.11	0.22
G2 20	49.38	2.03	14.74	12.40	0.12	7.63	11.42	1.96	0.12	0.21
G2 10	48.92	2.20	14.80	12.22	0.20	7.62	11.79	1.96	0.14	0.14
G2 32	49.46	2.33	14.76	11.75	0.10	7.61	11.62	1.92	0.20	0.24
G2 7	49.17	2.28	14.67	11.99	0.19	7.60	11.61	2.01	0.22	0.28
G2 24	49.51	2.04	14.80	12.56	0.23	7.59	11.09	1.88	0.11	0.18
G2 13	49.01	2.26	14.53	12.26	0.22	7.58	11.93	1.91	0.13	0.17
G2 25	48.74	2.77	14.48	13.13	0.21	7.57	10.78	1.95	0.19	0.19
G2 21	48.78	2.27	14.81	12.75	0.16	7.56	11.61	1.87	0.11	0.08
G2 26	48.57	2.33	14.56	13.16	0.25	7.56	11.46	1.85	0.12	0.15
G2 9	49.17	2.09	14.87	12.60	0.19	7.54	11.30	1.89	0.13	0.21
G2 31	49.47	2.47	14.54	11.88	0.16	7.54	11.84	1.83	0.10	0.18
G2 22	49.05	2.03	14.67	12.94	0.14	7.53	11.26	1.99	0.17	0.21
G2 27	49.44	2.14	14.88	12.40	0.22	7.51	11.17	1.97	0.12	0.16
G2 14	49.35	2.07	14.86	12.77	0.20	7.50	11.11	1.90	0.09	0.16
G2 23	49.30	2.12	14.79	12.77	0.17	7.48	11.27	1.92	0.10	0.09
G2 29	49.37	2.03	14.89	12.55	0.22	7.45	11.28	1.97	0.08	0.17
G2 24	49.04	2.27	14.45	12.65	0.18	7.45	11.80	1.84	0.19	0.14
G2 15	48.66	2.27	14.48	12.88	0.13	7.42	11.86	1.92	0.18	0.20
G2 19	48.53	2.42	14.35	12.67	0.17	7.40	12.42	1.77	0.22	0.05
AVER	**49.00**	**2.20**	**14.85**	**12.35**	**0.17**	**7.77**	**11.37**	**1.98**	**0.13**	**0.19**

Pillow-rim glass sample analyses (G4)

Sample	SiO_2	TiO_2	Al_2O_3	FeO	MnO	MgO	CaO	Na_2O	K_2O	P_2O_5
G4 12	46.96	2.21	15.54	11.81	0.14	9.06	11.29	2.74	0.19	0.06
G4 30	50.52	1.85	16.40	10.10	0.20	8.77	9.63	2.39	0.11	0.03
G4 24	47.86	2.26	15.50	12.11	0.07	8.71	11.03	2.32	0.11	0.05
G4 25	47.85	2.31	15.19	12.44	0.19	8.25	11.36	2.17	0.14	0.11
G4 38	50.58	1.90	15.59	11.03	0.18	8.23	10.11	2.13	0.22	0.03

G4 1	48.91	2.12	14.73	12.25	0.13	7.71	11.90	1.91	0.17	0.17
G4 19	48.71	2.23	15.02	12.06	0.16	7.70	12.01	1.86	0.08	0.18
G4 28	49.74	2.03	15.05	11.73	0.21	7.67	11.24	1.97	0.13	0.23
G4 33	49.15	2.15	15.02	12.34	0.14	7.67	11.19	1.97	0.12	0.26
G4 4	49.36	2.09	14.80	11.99	0.17	7.65	11.58	1.99	0.18	0.20
G4 12	49.78	1.91	15.18	11.66	0.20	7.65	11.20	1.96	0.16	0.31
G4 26	49.43	2.09	15.09	12.31	0.20	7.65	10.94	1.97	0.11	0.23
G4 35	50.04	2.32	14.88	11.31	0.13	7.60	11.27	1.99	0.16	0.30
G4 23	48.58	2.30	14.45	12.46	0.23	7.58	12.14	1.87	0.16	0.23
G4 5	49.13	2.27	14.89	11.90	0.20	7.53	11.75	1.92	0.18	0.25
G4 5	49.13	2.27	14.89	11.90	0.20	7.53	11.75	1.92	0.18	0.25
G4 14	49.14	2.36	14.82	11.89	0.15	7.51	11.80	1.94	0.16	0.23
G4 2	48.86	2.19	14.83	12.63	0.27	7.49	11.51	1.95	0.13	0.13
G4 3	48.64	2.08	14.60	13.49	0.27	7.48	11.33	1.90	0.09	0.12
G4 36	48.33	2.37	14.08	12.92	0.11	7.45	12.38	1.85	0.20	0.32
G4 37	48.85	2.31	14.80	12.26	0.19	7.44	12.05	1.87	0.19	0.05
G4 32	49.21	2.14	14.79	12.47	0.16	7.44	11.55	1.89	0.17	0.20
G4 34	48.37	2.04	14.46	13.25	0.24	7.43	12.01	1.91	0.17	0.12
G4 29	49.88	1.98	14.97	12.24	0.16	7.42	11.12	1.96	0.09	0.17
G4 27	48.91	2.13	14.70	12.64	0.18	7.40	11.77	1.85	0.21	0.21
G4 40	48.36	2.37	15.08	12.87	0.24	7.40	11.16	2.06	0.26	0.19
G4 16	48.13	2.39	14.22	13.17	0.19	7.36	12.25	1.85	0.18	0.27
G4 39	48.86	2.17	14.75	12.93	0.31	7.35	11.39	1.97	0.09	0.18
G4 17	48.61	2.29	14.45	13.30	0.11	7.33	11.67	1.96	0.15	0.13
G4 21	48.60	2.14	14.87	13.04	0.19	7.07	12.03	1.87	0.13	0.06
AVER	**48.95**	**2.17**	**14.92**	**12.28**	**0.18**	**7.68**	**11.48**	**2.00**	**0.15**	**0.17**

Interstitial glass analyses (G4 and K4)

Sample	SiO_2	TiO_2	Al_2O_3	FeO	MnO	MgO	CaO	Na_2O	K_2O	P_2O_5
G4M39	51.95	2.02	17.49	13.09	0.11	2.73	8.87	3.25	0.35	0.14
K4 29	52.08	4.50	10.25	13.39	0.24	2.83	13.97	2.02	0.35	0.37
K4 3	62.03	1.73	14.25	9.54	0.20	0.82	6.35	4.23	0.61	0.25
K4 14	65.24	2.42	13.28	7.66	0.22	0.39	4.94	3.84	1.27	0.75

Compositinal range of the pillow glass is large as compared with the whole-rock composition. The highest MgO content of the glass is lower than that of the MgO-richest whole-rock sample but the downward MgO range is large.

In Figure 17 the MgO-CaO relations of the glass are shown to reach down to values that corresponds to dacitic rocks. However, as clearly seen in Figure 17 the rim glasses are mostly between 7 and 9 Wt % MgO. Also seen in the Figure is the negative covariation of MgO and CaO in the upper right. This reflects a significant olivine control within the pillow glass during formation of the rims.

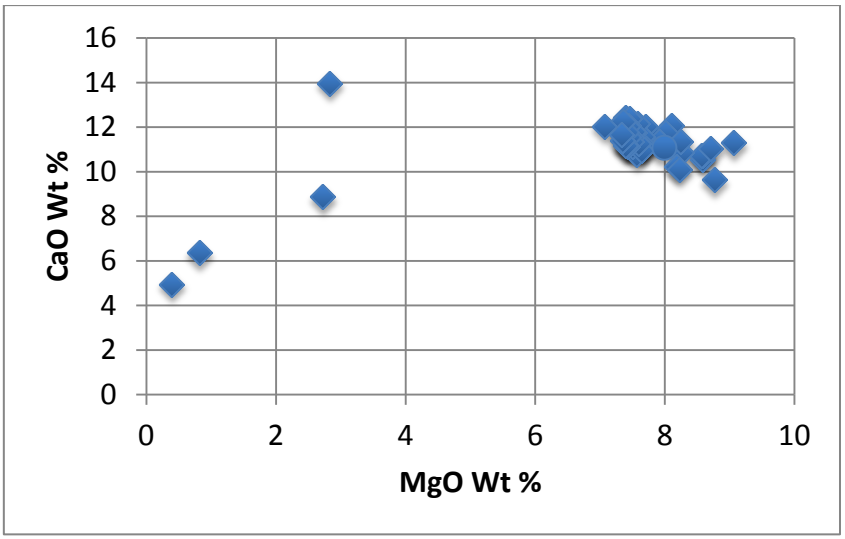

Figure 17. MgO-CaO relations of pillow glass. Note the point-cluster in the upper right where all the rim samples plot within a narrow range. The points to the left in the Figure denote the more evolved interstitial glass. Crystal fractionation would, indeed, move the composition from right to the left in the Figure.

3.3 Chemical composition of minerals

The mineralogy of the pillows was describes in the petrography chapter. In addition to chromite microphenocrysts, olivine phenocryst, plagioclase microphenpcrysts, oxide microphenocrysts and skeletal plagioclase nuclei are found in the glass. Clinopyroxenes were found in the transection away from the glassy rim, through the crust into the holocrystalline core. Titanomagnetite appears in the crust but is more abundant in the in the pillow core. Detailed microbeam analysis by EDS was made on these crystals to cast a light on how they developed over time.

3.3.1 Olivine

Analyses of olivine from pillow No. 4 are listed in Table 4. Total iron in Olivine from the pillow rim (G4) is from 14.46 to 16.07 Wt%, and Mg is from 44.79 to 46.34 Wt%. Samples from the pillow core are significantly higher in Fe (14.80 – 25.47 Wt%) and similarly lower in Mg (37.23 – 46.45 Wt%).

Table 4. Microbeam chemical analyses of olivine minerals.

Sample	SiO_2	FeO	MnO	MgO	SUM	% Fo
G4 1	38,83	14,76	0,13	46,28	100	84,8
G4 3	38,04	15,41	0,21	46,34	100	84,3
G4 4	39,02	16,07	0,13	44,79	100	83,3
G4 11	39,93	14,46	0,24	45,38	100	84,8
G4 20	38,46	15,76	0,20	45,57	100	83,8
K4 19	36,84	16,48	0,24	46,44	100	83,4
K4 20	36,40	16,89	0,26	46,45	100	83,1
K4 21	36,82	25,47	0,49	37,23	100	72,3
K4 22	37,80	21,54	0,24	40,42	100	77,0
K4 24	38,80	15,57	0,28	45,36	100	83,9
K4 25	39,58	14,80	0,27	45,36	100	84,5
K4 33	38,98	15,34	0,15	45,53	100	84,1

The end members of the olivine series are Mg_2SiO_4, fosterite and Fe_2SiO_4, fayalite, and there is complete solid solution between these extremes. This means that Mg^{2+} can be replaced in any proportion by Fe^{2+} in the olivine structure because these elements have similar ionic radii, Mg^{2+}= 0.72 Å and Fe^{2+}= 0.78Å (Klein and Dutrow, 2008).

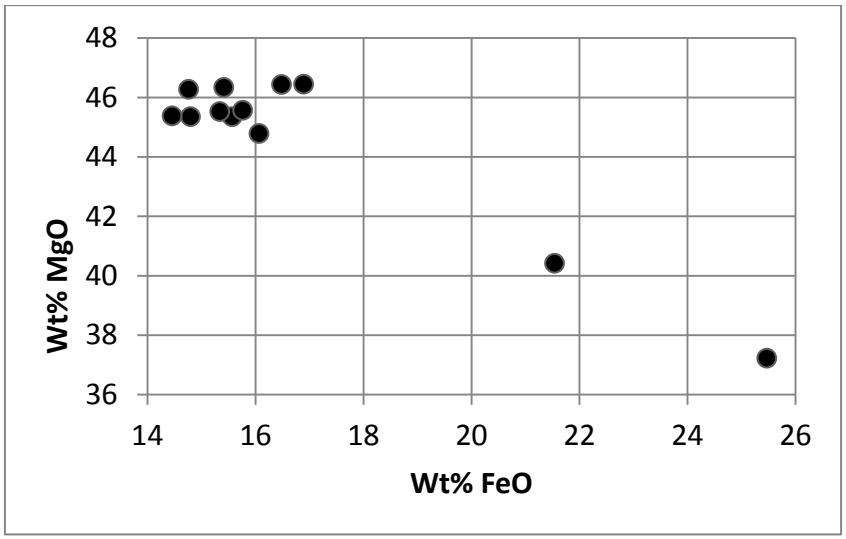

Figure 18. MgO and FeO in olivine crystals. Note that the majority of analyzed olivine crystals are almost identical in composition. The cluster in the upper left of the Figure probably contains the olivine phenocrysts that existed before the eruption.

In Figure 18 the negative correlation between Mg and Fe in olivine reflects a large variation in the liquid composition during crystallization. Most of the samples are within the same range in Mg and Fe (to the upper left in Figure 18). Two samples from the pillow core, No 21 and 22 are significantly evolved towards higher fayalite component indicating extensive fractionation during formation of the pillow.

At equilibrium, quartz is incompatible with Mg-rich olivine since it would have combined with olivine in to produce low calcium pyroxene. However, in some later-stage Fe-rich olivines coexist with quarts (Gribble and Hall, 1992). It is interesting in this context that moderately evolved olivine (Fo72) coexists with dacitic glass intergranular between plagioclase and clinopyroxene in the pillow cores. This implies that pervasive mineralogical equilibrium broke down towards the end of solidification.

3.3.2 Plagioclase

As evident from the petrographic study, the plagioclase in the outer pillow rims occurs as very small nuclei of bytownite. There is no doubt that the magma was saturated with respect to plagioclase during eruption and accordingly the largest plagioclase crystals of the pillow rim may be derived from pre-eruptive equilibrium with liquid and olivine.

Plagioclase analyses from pillow rim No. 4, have Ca from 11.92 Wt% to 17.97 Wt% and Na from 1.29 Wt% to 3.76 Wt%. This corresponds to an evolution from bytownite An88 to labradorite An63, actually close to the entire evolution range of rift-zone tholeiites.

Minerals from core samples (pillow No. 4 and 1) have Ca from 12.49 Wt% to 18.08 Wt%, and Na from 1.66 to 3.97 Wt% (Table 5). Evidently, the core may contain all types of minerals that crystallized during the formation of a pillow. It is tentatively concluded that most of the mineralogical evolution of a pillow takes place during formation of the crust as shown by the variable plagioclase composition with the glassy rim and the outer margin of the crust.

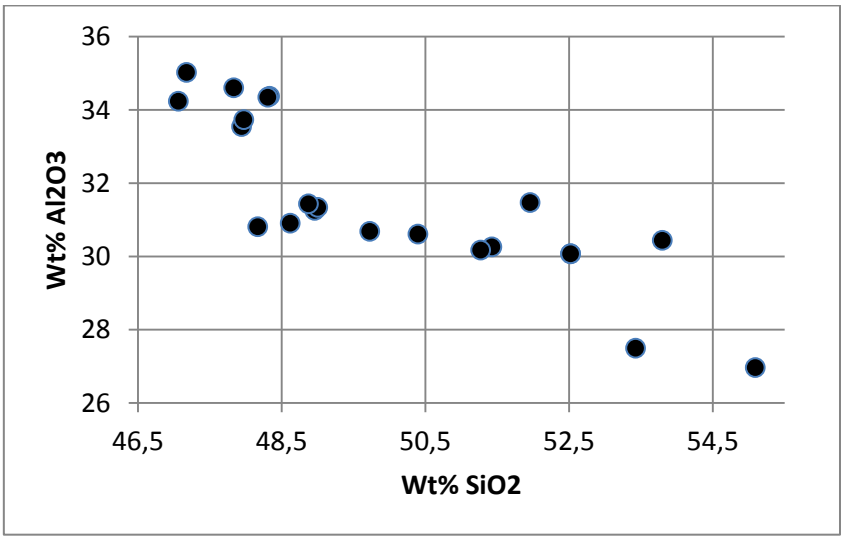

Figure 19. Al_2O_3 and SiO_2 relation in plagioclase, reflecting Al-Si substitution.

In feldspars, Al^{3+} substitutes for Si^{4+} in the framework structure where coupled substitution is required to maintain charge balance (Klein and Dutrow, 2008). Figure 19 shows strong negative linear relationship between Al and Si in plagioclase that represent the entire range of compositions across a glassy rim into the pillow crust. The group of bytownite in the upper left of the Figure may, indeed, represent the plagioclase composition that existed at constant temperature prior to eruption while the trend towards lower Al was formed during cooling and crystallization of the pillow rim and outer crust.

Table 5. Microbeam chemical analysis of plagioclase minerals.

Sample	SiO_2	Al_2O_3	CaO	Na_2O	K_2O	sum	% An
G4 12	47,94	33,55	17,20	1,29	0,02	100	88,1
G4 13	48,33	34,38	15,45	1,83	0,01	100	82,4
G4 14	47,97	33,73	16,27	1,97	0,05	100	82,0
G4 15	47,83	34,60	15,79	1,73	0,05	100	83,5
G4 22	52,52	30,07	14,44	2,91	0,06	100	73,3
G4 22	52,52	30,07	14,44	2,91	0,06	100	73,3
G4 25	48,31	34,35	15,31	2,03	0,00	100	80,6
G4 28	47,06	34,24	16,98	1,71	0,01	100	84,6
G4 29	53,42	27,50	15,73	3,35	0,00	100	72,2
G4 31	48,87	31,44	17,56	2,10	0,03	100	82,2
G4 32	48,62	30,91	17,97	2,45	0,05	100	80,2
G4 36	51,27	30,18	16,07	2,47	0,02	100	78,2
G4 41	55,09	26,97	14,32	3,55	0,07	100	69,0
G4 42	51,96	31,47	13,25	3,30	0,02	100	68,9
G4 43	53,80	30,44	11,92	3,76	0,07	100	63,7
G4 44	47,18	35,03	15,79	1,98	0,02	100	81,5
K4 5	51,43	30,26	12,49	3,97	0,09	98,24	63,5
K4 15	48,17	30,81	17,81	2,33	0,00	99,12	80,9
K4 17	48,96	31,26	18,08	1,66	0,04	100	85,8
K4 18	50,40	30,61	15,73	3,24	0,03	100	72,8
K1 4	49,73	30,69	15,69	2,73	0,09	98,92	76,1
K1 2	49,00	31,34	16,13	2,27	0,09	98,84	79,7

3.3.3 Pyroxene

Unfortunately, many of the chemical analyses of the pyroxenes in the study were obscured by other phases in the surroundings. The reason is the small crystal size of interstitial pyroxenes that form towards the end of crystallization (Figure 9). The few acceptable analysis are from the core of pillows No. 1 and 4.

Calculations of % En, % Wo, and % Fs reveal almost constant %Fs and only slight variation in %Wo and % En, all crystals being augite

Table 6. Microbeam chemical analyses of clinopyroxene minerals.

Sample	SiO_2	TiO_2	Al_2O_3	FeO	MnO	MgO	CaO	SUM	% En	% Wo	% Fs
K4 4	45,58	4,30	5,89	15,69	0,29	9,65	18,28	100	30,5	41,6	27,9
K1 5	45,56	5,26	6,27	14,10	0,23	8,85	19,34	100	28,9	45,3	25,8
K1 6	45,57	5,20	6,44	14,30	0,33	8,93	18,71	100	29,4	44,2	26,4
K1 7	47,53	2,11	3,72	16,37	0,38	10,03	19,47	100	30,2	42,1	27,7
G4 40	45,34	2,86	12,37	13,82	0,24	11,12	13,55	100	38,9	34,0	27,1

One pyroxene analysis from the pillow rim (G4 40) is far from the others chemically, with Mg 11.12 Wt%, Fe 13.82 Wt%, and Ca 13.55 Wt%, while the others are lower in Mg (8.85 Wt% to 10.03 Wt%), higher in Fe (14.10 Wt% to 16.37 Wt%), and higher in Ca (18.28 Wt% to 19.47 Wt%). This sample is the one to the left in Figure 20.

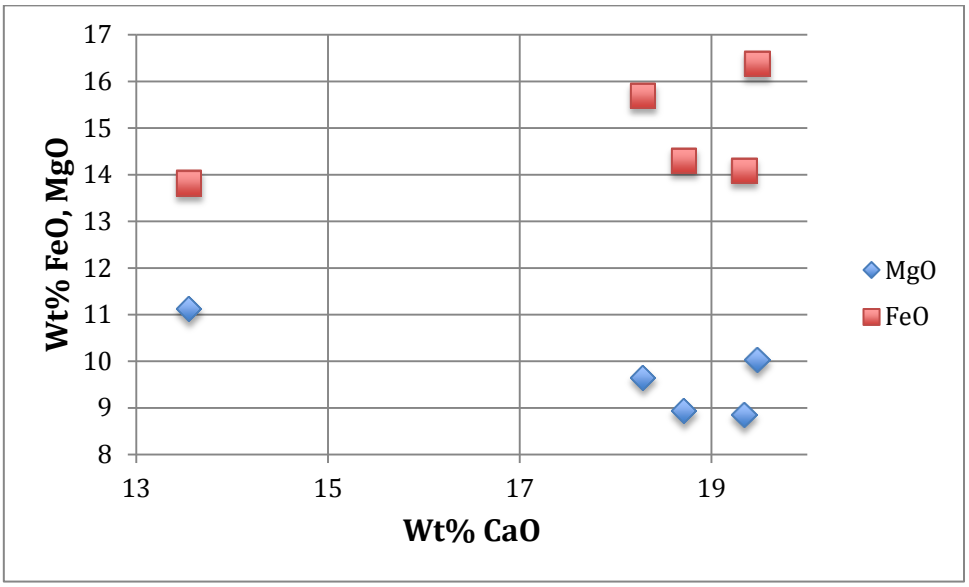

Figure 20. MgO, FeO and CaO relations in clinopyroxene.

In Figure 20 a positive correlation is observed between Fe and Ca while negative correlation is observed between Mg and Ca. The Figure, therefore, reveals a slight substitution between of Fe for Mg.

Superimposed on the narrow compositional range of Ca, Fe and Mg is a bimodal distribution of Ti outlined in the petrography section where two generations of augite are noticed. The important differences among the pyroxenes regards the Ti-content. At similar major-oxide the TiO_2 content falls into two ranges, about 2-3 Wt% and about 4-5 Wt%. The occurrence of these groups is clearly distinct; the high Ti-augite forms first before the occurrence of titanomagnetite and the commom augite forms in equilibrium with titanomagnetite. This scenario may be seen in Figure 9 where Ti-augite lists are simply terminated by newly nucleated titanomagnetite. As seen in the high TiO_2 content (5 Wt%) of the intermediate interstitial glass and the low TiO_2 content of the silicic glass (Table 3), a significant shift in TiO_2 content of the melt occures during the late crystallization of the pillow core.

3.3.4 Oxides

Oxides are minerals that contain one or more metals and oxygen. The Fe-Ti oxides often occur widely in rocks of all types, frequently as submicroscopic intergrowths, which result from cooling and oxidation. Chemical substitution of Cr, Mn, Mg, and Al is extensive in the cubic oxides, therefore, precise identification can be difficult. In typical basaltic igneous rocks there are two primary oxide minerals, ilmenite and titanomagnetite (Gribble and Hall, 1992) while chromite and chromian spinel are abundant in mantle derived rocks. Chemical analyses from rim and core samples (pillow No. 4) were divided up in two

tables; Table 7 showing analyses of chromite and Table 8 showing analyses of titanomagnetite.

Analysis of the almost homogeneous chromite microphenocrysts are listed in Table 7. Crystal from the pillow core sample K4 35 in Table 7 is, however, significantly higher in Ti (10.44 Wt%) and Fe than the rest of the chromite (1.63 Wt% to 2.50 Wt% Ti), but still not high enough to classify as titanomagnetite. It may be inferred that that this composition represents titanomagnetite that was nucleated upon a prexisting spinel nudget in the core of the pillow. There is no compositional difference between chromite inclusions in olivine and chromite microphenocrysts. Therefore, it is concluded that the chromite is a mantle derived phenocryst.

Table 7. Microbeam chemical analyses and end members of chromite minerals in basaltic pillow No. 4.*

Sample:	K4 3	K4 35	K4 36	G4-5	G4-7	G4-8	G4-9	G4-16	G4-26
TiO_2	2.50	10.44	2.17	1.87	1.63	1.76	1.74	2.37	2.22
Al_2O_3	22.33	9.98	23.17	22.68	23.58	19.78	23.36	20.27	21.47
Cr_2O_3	34.52	20.96	33.07	36.72	38.45	40.43	35.07	37.13	35.25
FeO	29.62	54.65	30.14	27.18	24.50	27.58	28.76	29.70	30.30
MnO	0.24	0.28	0.21	0.24	0.12	0.12	0.07	0.36	0.17
MgO	10.79	3.70	11.24	11.31	11.71	10.33	11.01	10.17	10.58
Mol%									
Chr	0.43	0.27	0.40	0.45	0.47	0.50	0.43	0.46	0.44
Herc		0.01							
Mt	0.1	0.26	0.12	0.09	0.07	0.07	0.1	0.10	0.12
Sp	0.5	0.19	0.52	0.53	0.54	0.49	0.51	0.48	0.49
Usp	0.06	0.26	0.05	0.04	0.04	0.04	0.04	0.06	0.05

*http://melts.ofm-research.org/CalcForms/spinel.html

Molecular composition of the chromites in Table 7, calculated according to Sack and Ghiorso (1991a) and Sack and Ghiorso (1991b) shows almost constant chromite spinel ratio with the exception of sample K4 35.

All the virtually identical titanomagnetites are from the pillow core (Table 8), and have Ti from 20.88 Wt% to 24.62 Wt%. corresponding to 59-70 Wt% ulvospinel. This means that the titanomagnetites are nucleated at very similar temperatures and similar magmatic conditions.

Table 8. Microbeam chemical analyses of titanomagnetite minerals from basaltic pillow No 4. Wt % Usp is calculated according to Lepage (2003).

Sample	TiO_2	Al_2O_3	FeO	MnO	MgO	%Usp
K4 6	22.19	3.10	73.85	0.57	0.28	63
K4 10	21.61	2.17	75.24	0.58	0.39	61
K4 11	24.62	2.77	71.73	0.59	0.29	70
K4 1	21.52	3.31	74.09	0.44	0.64	61
K4 2	20.88	2.48	75.83	0.40	0.42	59

The tianomagnetite is regular in composition indicating buffered oxygen fugacity during its formation. Recalling the FeO analysis of the whole rock samples (Table 2) and the positive correlation of Fe(III) and total iron it may be assumed, however, that the oxygen fugacity of the samples was somewhat variable.

Equilibrium calculation at FMQ oxidation state in the COMAGMAT software shows that the whole rock sample (K4, Table 2.) has liqudus temperature of 1195 °C assuming 100 bar pressure and 0.2 Wt % H_2O content. Calculated oxygen fugacity exponent –8.33, corresponds to FeO/Fe-tot ratio at 0.881.

The analyzed FeO/Fe-tot ratio of this sample is also 0.881 which confirms that this sample is on the FMQ-oxygen buffer. A slight deviation from this oxidation stage (Table 2) in other samples is due to different amount of olivine and plagioclase in the rock. The more fractionated, iron rich samples appear more oxidized simply due to lower olivine content.

This scenario is a typical closed system evolution with respect to oxygen, excluding local oxidation from the steam-dominated surroundings. This finding confirms that the pillow samples perfectly preserve their primary oxidation state.

4 Disscussion

For the purpose of collecting a representative sample of a basaltic pillow that truly represents its source-magma the chemical variation within a pillow has to be defined. This is evidently a complicated task. A pillow outcrop such as the Armannsfell road-cut may show a range in whole rock analysis that can be correctly placed within a certain rock suite but its original magmatic composition may be obscured by internal fractionation. This problem is illustrated in Figure 21 where the Armannsfell samples define a trend among samples from the WRZ and the Reykjanes Peninsula.

The Hengill center volcano is on the southwest margin of the WRZ, and has produced about 25-30km^3 of hyaloclastite and lava during the last 0.11 million years (Tronnes, 1990; Hansteen, 1991). The Hengill rock suite has bimodal composition; High-Mg primitive group in the central graben of the WRZ and High-Ti group occurring along the western margin of the WRZ. Based on whole rock analysis the Armannsfell basalt may be assumed to be characteristic for the westen rift-zone margin.

Pillow basalt samples from Armannsfell show high TiO_2 compared to postglacial lava units in the WRZ central graben (Sinton et. al., 2005) and, therefore, do not belong to the same petrochemical trend.

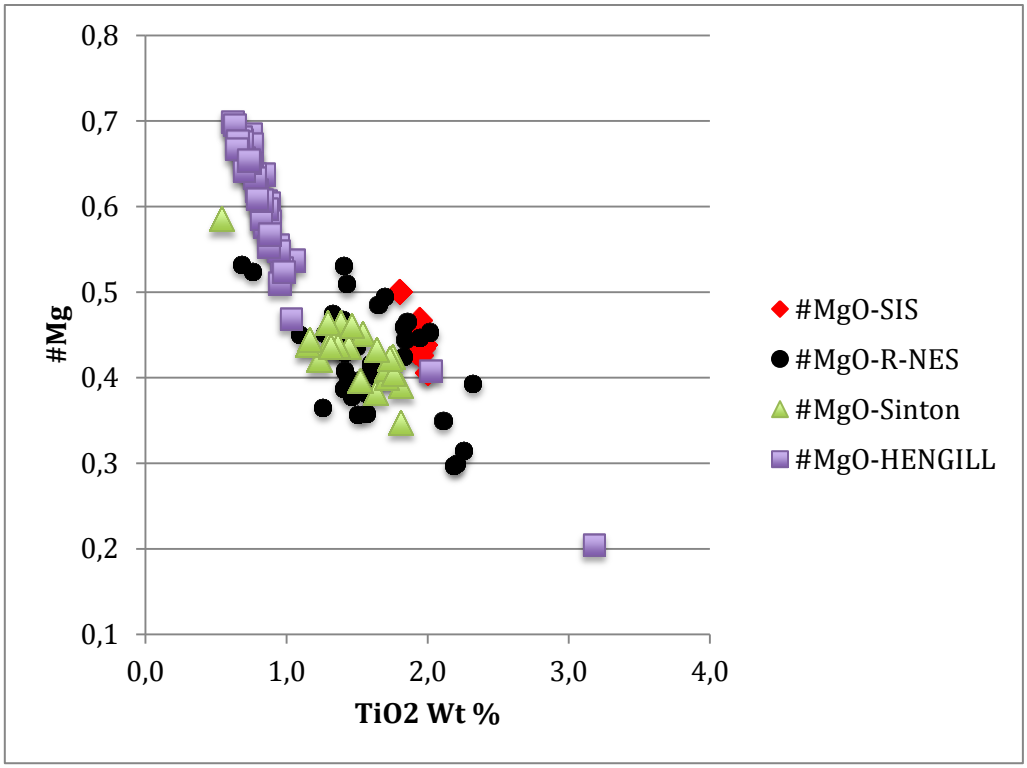

Figure 21. Magnesium number and titania relations of the Armannsfell pillows in relation to rocks from the Western rift zone, Hengill and the Reykjanes Peninsula (R-NES). The Armansfell pillows (#MgO-SIS) fall among rocks from western margin of the WRZ.

Pillows from Ármannsfell were also compared to analyses from Reykjanes Peninsula, (Data from the Geochemical data bank of the Institute of Earth Scienses) (Figure 21). The samples from the Reykjanes Peninsula show the same bimodality as the Hengill samples and Armannsfell clearly belongs to the High-Ti trend.

Figure 21 clearly illustrates the question addressed in the present contribution: What information can be expected from a single sample of a basaltic pillow or a sample of individual pillow rim? In the Quaternary subglacial basalt formation of Iceland, isolated pillow fragments are often the only fresh rock samples available. An even more critical sampling environment is the dredging of pillow fragments from the ocean floors. The present conclusion is that although analysis of singular basaltic pillow fragments may place the rock within a correct petrochemical trend the precise magmatic composition may remain unknown.

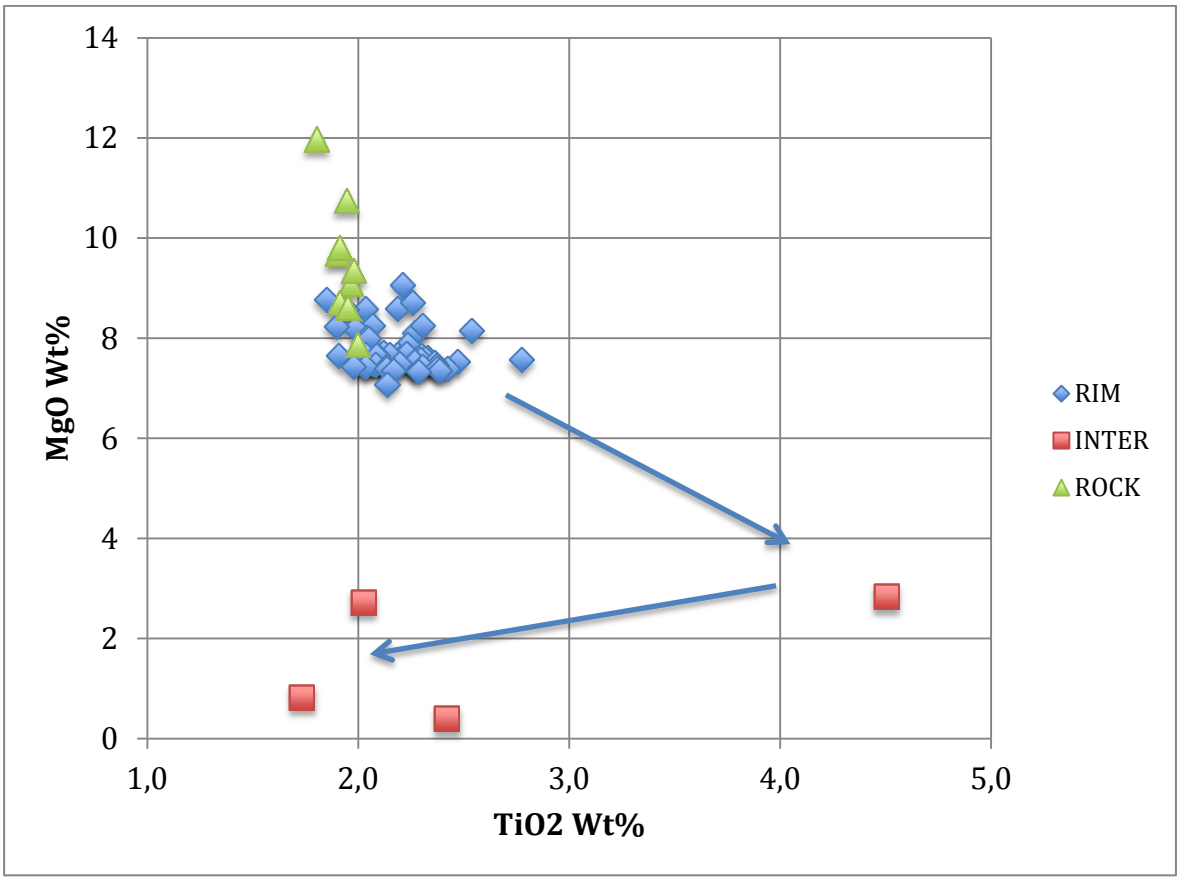

Figure 22. MgO-TiO_2 relations of whole rock and glass analyses. Blue diamonds denote rim glass, red squares denote interstitial core glass and green triangles indicate whole rock samples. Arrows indicate assumed fractionation trend.

The chemical range of the Armannsfell whole rock analys and the pillow fragments is shown in Figure 22. It is obvious that while the whole rock analysis form a trend that may result from crystal fractionation or control during pillow formation most of the rim glass defines a narrow cluster. Interstitial core-glass analysis form a line of descent from the rim glass, reaching dacitic composition before quenching. The fractionation trend is indicated by arrows in Figure 22.

It is not unexpected that the crystallization of olivine tholeiite can display the entire petrochemical range of the Icelandic rift zones. However, the fact that the fractionation process takes place on a time scale of minutes is remarkable and casts some doubts on the significance of pillow samples for reconstruction of initial magmatic compositions. In terms of volume, a pillow rim is a small part of a pillow. As stated earlier, the crust and the core make up most of the pillow section. In Table 2 it was shown that the normative composition of the whole rock samples is somewhat variable. In Table 4 the normative composition of pillow glass is outlined for few samples that cover the entire compositional range.

Table 9. Normative composition of pillow glass.*

Sample	G2 19b	G2 19a	K4 3	G4 4	G4 40	G4 39	G2 19	G4M39	AV
SiO2	47.90	48.95	50.57	49.22	52.01	52.13	62.10	65.30	49.03
TiO2	2.26	2.12	1.85	2.09	2.03	4.51	1.73	2.42	2.19
Al2O3	15.51	14.75	16.42	14.88	17.51	10.26	14.26	13.29	14.87
FeO	12.12	12.26	10.11	12.62	13.10	13.41	9.54	7.66	12.39
MnO	0.07	0.13	0.20	0.19	0.11	0.24	0.20	0.22	0.18
MgO	8.72	7.72	8.78	7.55	2.73	2.83	0.82	0.39	7.69
CaO	11.04	11.92	9.64	11.31	8.88	13.98	6.36	4.94	11.43
Na2O	2.22	1.81	2.29	1.79	3.15	1.92	4.13	3.74	1.88
K2O	0.11	0.17	0.11	0.13	0.35	0.35	0.61	1.27	0.14
P2O5	0.05	0.17	0.03	0.22	0.14	0.37	0.25	0.75	0.19
SUM %	100	100	100	100	100	100	100	100	100
NORM*									
Quartz	0.00	0.00	0.00	0.00	3.22	9.80	17.79	26.18	0.00
Plag	50.82	46.94	53.58	47.33	59.26	34.59	53.52	47.37	47.63
Orthocl	0.65	1.00	0.65	0.77	2.07	2.07	3.60	7.51	0.83
Diopside	18.39	21.78	10.96	18.59	9.01	41.30	9.91	3.41	19.59
Hypersth	11.59	21.89	29.03	27.74	21.30	1.82	10.60	8.61	24.13
Olivine	13.23	3.05	1.44	0.15	0.00	0.00	0.00	0.00	2.28
Ilmenite	4.29	4.03	3.51	3.97	3.86	8.57	3.29	4.60	4.16
Magnetite	0.97	0.99	0.81	1.01	1.06	1.09	0.77	0.62	1.00
Apatite	0.12	0.39	0.07	0.51	0.32	0.86	0.58	1.74	0.44

*Kurt Hollocher, Geology Department, Union College, Schenectady, NY, 12308, hollochk@union.edu

All samples listed have hypersthene in the norm which underlines the common tholeiitic character of the glass-suite. The most magnesian samples with the highest ol in the norm are to the left in the Table and the samples show evolution-on towards qz-tholeite and further evolution towards dacite listed to the right in the Table. The last column of the Table lists the average glass composition of the Armannsfell pillows (Sample AV). It is important to note that the average glass is very different from the whole rock analysis in Table 2. Only the most magnesian glasses to the left in Table 4 match the normatic olivine content of the whole rock samples.

In Fgure 23 the nornative composition of all samples is plotted in terms normative olivine and normative quarz. There is a striking difference between the whole rock analyses and majority of the glass analyses. However, few glass analyses match the whole rock composition and there is no doubt that the initial magmatic composition has to be sought within this group of whole rock samples and pillow-glasses.

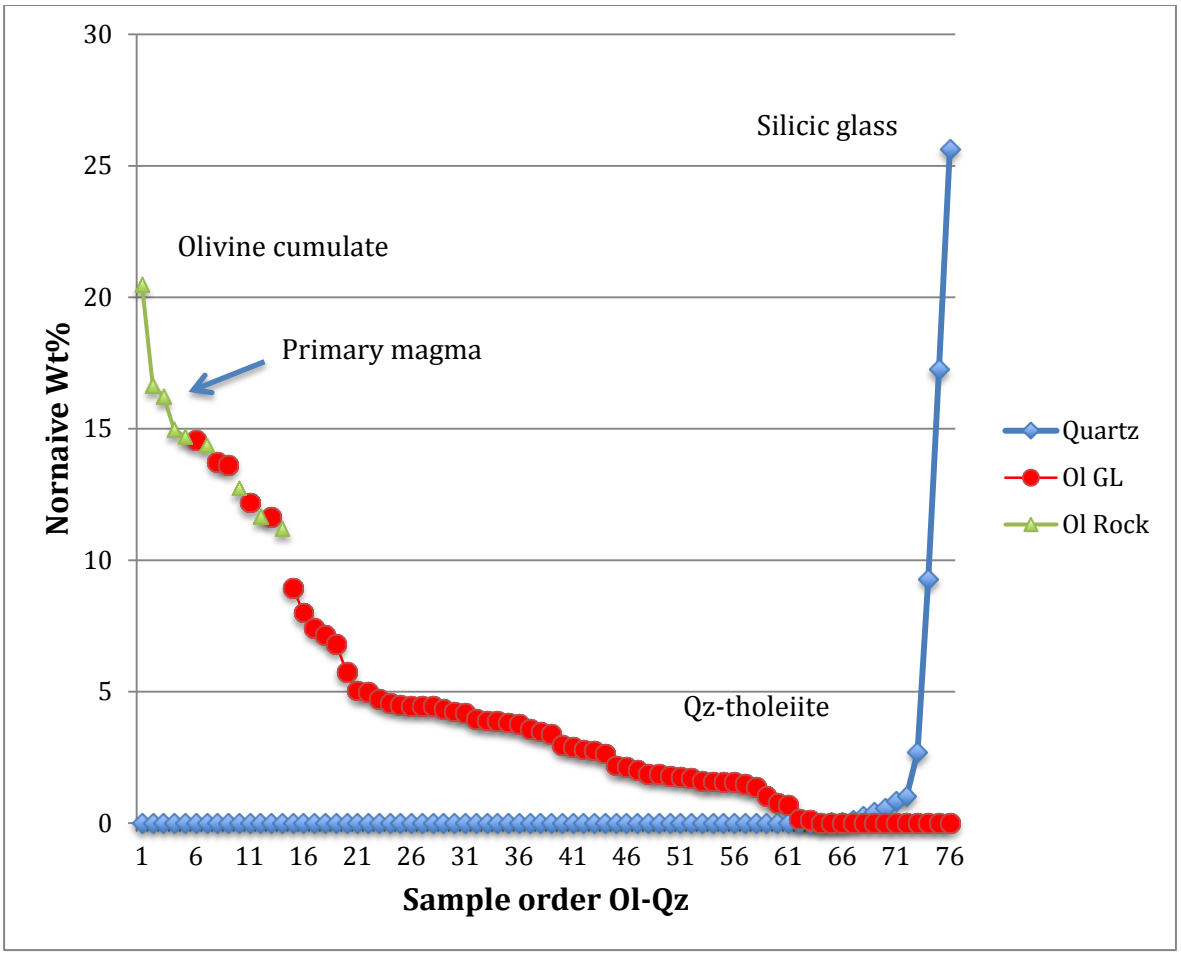

Figure 23. Normative ol and qz in glass from Armannsfell ordered from left to right by dereasing ol-content and incrasing qz-content. Blue diamonds denote qz-normative compositions, red dots denote ol-normative glass compositions and green triangles indicate the whole rock samples (Table 2). Inferred primary magma, olivine cumulate, qz-tholeiite and silicic glass are marked in the Figure.

Primary composition of the pillow-basalt is evidently slightly more primitive (magnesian) than the most magnesian glass. There is also little doubt that the most magnesian whole rock sample contains olivine cumulate (upper left in Figure 23).

It is, therefoe, concluded that the most likely primary composition of the pillow-basalt is found in two whole rock sample that plot slightly above the most magnesian glasses. Other whole rock samples are fractionated by olivine and plagioclase loss before their crystallization and they, therefore, fall within the composition of the most magnesian glasses.

As outlined earlier in this contribution the formation of basaltic pillow involves transport of magma into a cooling conduit where flow resistance increases by time. A tentative conclusion was that a representative composition of the magma can most likely be found in the core at the root of a pillow where new magma is supplied during the entire pillow formation.

It is, therefore, concluded that the Armannsfell magma is represented by the most magnesian whole rock analyses where olivine cumulation is absent. This implies that a meaningful sample of pillow basalt, in terms of its initial composition, can only be found by the analysis and evaluation of several samples, preferably of pillow cores.

5 Conclusions

Basaltic pillows form during channelled magma flow and rapid cooling that enforce continuous fractionation of the primary magma. The process involves mechanical flow-fractionation of pre-existing and newly formed crystals as well as closed-system crystal fractionation within stagnant domains within the pillow.

In the Armansfell pillows, euhedral unzoned olivine phenocrysts, occasional chromite microphenocrysts and homogeneous population of plagioclase microphenocrysts were the only minerals found in the pillow glass rim, indicating fast magma ascended that prevented significant crystal gowth during the ascent of the magma. Chemical and mineralogical evolution observed in the pillows is, therefore, assumed to take place during emplacement by rapidly cooling channelled flow of melt and phenocrysts. On the other hand, the abundant skeletal plagioclase aggregates and lists found in the glass indicate that the melt was saturated and that crystallization of the pillows proceeded very fast.

Microbeam analysis by EDS confirm that the olivines phenocryst in the pillow rim are unzoned. That shows that olivine and plagioclase are precipitating in cotectic relations resembling the Fo-An cotectic in the system Fo-Di-An.

Within the inwards margin of the pillow rim and within the pillow crust the dominating mineral is skeletal plagioclase and bytownite lists, which become larger towards the interior and in the core due to longer cooling time.

Clinopyroxene augite is the third mineral to form, first as Ti-augite feathers in between plagioclase lists but later as common augite after the fourth mineral, titanomagnetie, enters the mineral assemblage towards the end of crystallization.

A continuous flow differentiation and crystal growth fractionates the residual melt. At early stages the relatively large olivine phenocrysts tend to accumulate in the flowing core. The finalfractionation process takes place in stagnant domains of the pillow core leading to the formation of interstitial qz-tholeiitc- and intermediate to silicic glass in the pillow core.

A representative sample of pillow basalt can only be selected after analysis and comparison of several subunits of several pillows. The core section at the root of the pillow composed of the last magma injection is most likely to represent the unfractionated primary magma composition.

References

Andrade, S., Hypolito, R., Ulbrich, H. H. G. J., Silva, M. L., 2002. Iron II oxide determination in rocks and minerals. *Chemical Geology,* 182, 85–89.

Bouhifd, M. A., Besson, P., Courtial, P., Gérardin, C., Navrotsky, A., Richet, P., 2007. Thermochemistry and melting properties of basalt. *Contributions to Mineralogy and Petrology,* 153, 689– 698.

Govindaraju, K., Mevelle, G., 1987. Fully automated dissolution and separation methods for inductively coupled plasma atomic emission spectrometry rock analysis. Application to the determination of REE. *Journal of Analytical Atomic Spectrometry 2*, 615–621.

Cashman, K. V., 1993. Relationship between plagioclase crystallization and cooling rate in basaltic melts. *Contributions to Mineralogy and Petrology,* 113-142.

Gribble, C. D., Hall, A. J., 1992. Optical mineralogy: Principles & practice. NW USA, CRC Press.

Hansteen, T.H., 1991. Multistage evolution of the picritic Maelifell rocks, SW-Iceland - constraints from mineralogy and inclusions of glass and fluid in olivine. *Contributions to Mineralogy and Petrology,* 109(2), 225-239.

Hoskuldsson, A., 2013. Generation of pillow basalts in Iceland, submarine to subglacial. Paper presented at the *Scientific Assembly,* Kagoshima, 20th of July.

Jakobsson, S. P., Gudmundsson, M. T., 2008. Subglacial and intraglacial volcanic formations in Iceland. *Jokull,* 58, 179–196.

Klein, C., Dutrow, B., 2008. The manual of mineral science (23rd edition). Massachusetts, Jay O'Callaghan.

Lepage, L.D., 2003. ILMAT: an excel worksheet for ilmenite-magnetite geothermometry and geobarometry. Computures and Geosciences. 29 (5), 673-678.

Muller, G., 1998. Experimental simulation of basalt columns. *Journal of Volcanology and Geothermal Research*, 86, 93–96.

Munchill, E. G., Lasaga, A. C., 1987. Crystal-growth kinetics of plagioclase in igneous systems: One-atmosphere experiments and application of a simplified growth model. *American Mineralogist,* 72, 299-311.

Nielsen, R., 2014. GERM Partition Coefficient (Kd) Database. Development and Maintenance by the EarthRef.org Database Team. Data contribution by Roger Nielsen. Retrieved from *http://earthref.org/KDD/*

Sack RO, Ghiorso MS (1991a) An internally consistent model for the thermodynamic properties of Fe-Mg-titanomagnetite-aluminate spinels. Contributions to Mineralogy and Petrology 106, 474-505.

Sack RO, Ghiorso MS (1991b) Chromian spinels as petrogenetic indicators: thermodynamic and petrologic applications. American Mineralogist 76, 827-847.

Tronnes, R. G., 1990. Basaltic melt evolution of the Hengill Volcanic System, SW Iceland, and evidence for clinopyroxene assimilation in primitive tholeiitic magmas. *Journal of Geophysical Research*, 95(B10), 15893–15910.

O'Hara, M. J., 1965. Primary magmas and the origin of basalts. *Scottish Journal Geology*, 1, 19–40.

Orlando, A., D'Orazio, M., Armienti, P., Borrini, D., 2008. Experimental determination of plagioclase and clinopyroxene crystal growth rates in an anhydrous trachybasalt from Mt Etna (Italy). *European Journal of Mineralogy*, 20(4), 653– 664.

Oskarsson, N., Sigvaldason, G. E., Steinthorsson, S., 1982. A dynamic model of rift zone petrogenesis and the regional petrology of Iceland. *Journal of Petrology*, *23*, 28–74.

Presnall, D. C., Hoover, J. D., 1984. Composition and depth of origin of primary mid-ocean ridge basalts. *Contributions to Mineralogy and Petrology*, 87, 170–178.

Rogan, W., Blake, S., Smith, I., 1996. In situ chemical fractionation in thin basaltic lava flows: examples from the Auckland volcanic field, New Zealand, and a general physical model. *Journal of Volcanology and Geothermal Research*, 74, 89–99.

Sinton, J., Gronvold, K., Sæmundsson, K., 2005. Postglacial eruptive history of the Western Volcanic Zone, Iceland. *Geochemistry, Geophysics, Geosystems*, 6(12), 1–34.

Sinton, J., 2009. Geological map of the Western Volcanic Zone, Iceland. Retrieved in the 8th March, 2013, from: *http://www.soest.hawaii.edu/GG/FACULTY/SINTON/Iceland/WVZ_Map.pdf*

Wilson, A. D., 1955. A new method for the determination of ferrous iron in rocks and minerals. *Bulletin of the Geological Survey of Great Britain*, 9, 56–58.

Winter, J.D., 2010. Principles of Igneous and Metamorphic Petrology (2nd edition): Metamorphic Facies and Metamorphosed Mafic Rocks. New Jersey, Pearson Education Inc.

Appendix A: Procedure for ICP-OES analysis

In this study, all samples were dissolved for ICP-analysis, to determine the bulk chemical composition. The analysis was based on the method from Govindaraju and Mevell (1978).

Sample preparation: Glass samples were prepared for dissolution by following steps.

1. Crushed with hammer.
2. Sieved (1 mm – 125 μm).
3. Magnet used to sort out the crystals from the glass (grain size from 250 to 125 μm.)
4. Glass particles washed and dried.
5. Further breakdown was done by electrical mortal.
6. Weighed in with lithium metaborat ($LiBO_2$) and fluxed in graphite crucible for 30 minutes at 1000°C.

Rock samples were prepared for dissolution by the following steps.

1. Crushed with hammer.
2. Broken down in a Platner mortal.
3. Further breakdown was done by electrical mortal.
4. Weighed in with lithium metaborat ($LiBO_2$) and fluxed in graphite crucible for 30 minutes at 1000°C.

Reference samples for instrument calibration were the "in house standards" A-THO, B-ALK and B-HTO. The unknown samples contained, 0.100 mg of rock/glass powder and 0.200 mg flux, to maintain constant rock/flux mass ratio of 2, while reference samples were made of 0.250 mg rock sample and 0.500 mg flux.

After melting, the resulting glass beds were dissolved with continuous agitation in 100 x its weight of acid mixture (0.30 mg for the unknowns, 0.75 mg for reference samples). The acid mixture is made of deionized water with vol 5% nitric acid, 1.33 vol % hydrochloric acid and 1.33 vol% semi-saturated oxalic acid ($H_2C_2O_4$).

Instrumental method

The chemical analyses were done at the Institute of Earth Sciences (University of Iceland) by SPECTRO-CIROS spectrometer. This spectrometer has Paschen-Runge setup, which

means that it can read all spectrolines at the same time. The light source in the spectrometer is argon plasma (inductively coupled plasma, ICP).

The dissolved samples were mixed with the gas as they were aspirated into a tiny ratio frequency generator, where the plasma was created. Each element has their own emission line, which is isolated by a diffraction grating and detected by series of photomultipliers, each on separate channel tuned for specific element (Winter, 2010). The analytical session starts with running of the three calibration standards, and each sample is measured in four 25 seconds reading sessions after 40 second flushing of the nebulizer with the sample itself. All channels are then simultaneously counted and fed to an on-board computer, where the SpectraVision software is used to calculate concentration of each element.

Appendix B: Procedure for Scanning Electron Microscope (SEM) and Energy Dispersive System (EDS) analysis

In this study samples from the pillow rim (G4), crust (M1) and core (K1) were analysed by SEM and EDS.

Sample preparation: Single glass/rock samples were handpicked from these samples, and sections were prepared for petrographic observations on a rounded microscope glass.

All samples were prepared for the analysis by following steps.

1. Glass/rock samples polished one by one.

2. Mounted into epoxy (important that the samples were completely dry) and left over night at 120°C, this was done so the epoxy can transform to a solid format.

3. Samples were polished, first with 800 grids sandpaper, and then with 2000 grids.

4. Coated with carbon.

Instrument method

The SEM and EDS analyses were done at the Institute of Earth Sciences (University of Iceland) by Hitachi Tabletop Microscope TM3000. This microscope has QUANTAX EDS and for the chemical analyses software from Burker Nano GmbH was used. Running conditions for microprobe analyses were 15kV accelerating voltage at 15nA bean current.

X-ray fluorescence is a sensitive technique for obtaining chemical analyses of bulk samples including low-abundance elements. The scanning electron microscope (SEM) provides image of crystal morphology and surface features of materials at the micrometer level, with a high intensity electron beam that is scanned across specific area. In the analysis volume, the incident higher-energy electrons displace inner-shell electrons, releasing energy by emission of X-rays of a wavelength characteristic of each element. The impact of an electron beam on the surface of a solid sample causes radiation signals, which includes BSE (backscattered electrons), secondary electrons, X-rays, cathodoluminescence radiation, and electrons adsorbed by the specimen (specimen current). Numerous detectors above the specimen record these signals, for example, one detector measures the intensity of the BSE which is related to the average atomic number of the specimen, its crystallographic orientation, and surface topography. Many SEM have energy-dispersive X-ray detection system (EDS), which allows for the spectral analysis of X-rays generated from the specimen directly under the electron beam. This technique provides chemical information that is generally sufficient for identification of an unknown. This addition to the SEM makes the composition information possible to detect, both rapidly and simultaneously from the same area (Klein and Dutrow, 2008).

Appendix C: The Wilson Method

Most chemical analyses of rocks and minerals done by modern instrumental methods like ICP-OES and EDS, calculate the total FeO. That means that they don't provide knowledge about the Fe(II)/Fe(III) ratio. The classical titration method is still the only one that can determine accurately the total amounts of Fe(II) and Fe(III) (Andrade et al., 2002). In this study Fe(II) determinations were performed on all samples with a modified version of the Wilson method (Wilson, 1955).

Procedure

The preparation of the samples, from glass and rock form to powder was the same as described in Appendix A.

The titration was done by the following steps.

1. 100±10 mg of the powdered glass and rock samples were weighted into a plastic container, to the fourth decimal point (Table 10).
2. Weighted samples were dissolved with 1 ml of HF, and 1 ml of V^{5+} in the plastic container, and the same was done for three blank samples. The samples were given almost 24 hours to stand until the decomposition of the rock powder was complete.

In the meantime, Fe (II) solution was prepared, from 9.8 g $(NH_4)_2Fe(SO_4)_2$ x $6H_2O$, 0.5 L of distilled water and a few drops of 1M H_2SO_4.

Then the Fe (II) solution was standardized with PH buffer that contained 0.5 ml of saturated H_3BO_3, 5ml of H_2SO_4, 2 drops of the indicator diphenylamine and 5.38 ml of $K_2Cr_2O_7$.

10.92 ml of the standardized Fe(II) solution were needed to get the reaction. Therefore, the normality of the solution is 0.04926N (5.38 ml x 10.92ml).

To know the maximum oxidation of vanadate, a titration was formed on a sample made up from the Fe(II) solution, 5ml of H_2SO_4, 1 ml of vanadate and 2 drops of diphenylamine. The result from this titration showed that 4.05 ml of the Fe(II) solution was needed to use up all the vanadate in the sample.

From this information it was possible to calculate the precent of FeO that uses up all the vanadate in the 100 mg sample (Table 10). Therefore, 14.35% FeO uses all the vanadate in 100 mg sample. The ICP-analyses showed that the most FeO in the samples are 12.25 mg (Table 2), this means that there is enough vanadate present for the Wilson titration.

3. After the samples had been dissolved, 50 ml of H_3BO_3 and 4 drops of diphenylamine were added to the plastic container.

4. Remaining V^{5+} of the solution was titrated using the standardized 1M Fe (II) solution. This titration was first done for the blank samples, the most successful one was 4.27 ml, and was used to determine the equilibrium, Table 10.

Table 10. Results from the Wilson titration and calculations.

Sample	Titration (ml)	Blank (ml)	Δml	Weight (mg)	meq FeO	mg FeO	%FeO	Fe_2O_3-asFeO	Fe_2O_3	%Fe(III)
G1	1,52	4,27	2,75	98,4	0,135	9,7213	9,879	1,94	2,154	16,41
M1	1,25	4,27	3,02	101,3	0,149	10,676	10,54	0,97	1,078	8,432
K1	1,57	4,27	2,7	91,68	0,133	9,5446	10,41	1,45	1,606	12,19
G2	1,49	4,27	2,78	93,25	0,137	9,8274	10,54	1,40	1,554	11,72
G3	1,66	4,27	2,61	91,78	0,128	9,2264	10,05	2,19	2,438	17,92
G4	1,48	4,27	2,79	92,78	0,137	9,8627	10,63	1,32	1,465	11,03
M4	1,38	4,27	2,89	101,2	0,142	10,216	10,1	1,49	1,653	12,84
K4	1,4	4,27	2,87	98,49	0,141	10,146	10,3	1,19	1,319	10,33
G5	1,23	4,27	3,04	108,1	0,15	10,746	9,939	1,88	2,089	15,91

Wilson titration method

After the dissolution of powdered samples, the most frequent change is the oxidation of Fe(II) to Fe(III). The presence of fluorides enhances the reaction by decreasing the redox potential of the system Fe(II)/Fe(III) from 0.77 to about 0.1 V. Therefore, a recommended procedure would be to form the dissolution in an inert atmosphere, but that is not easy and may not even be very effective in preventing oxidation. The oxidation effect can be monitored in a better way by triggering the oxidation reaction with the addition of a large known amount of an oxidizing agent. In this way the ferrous ions can pass immediately into the ferric state during the dissolution, thus avoiding secondary reactions such as oxidation by air (Andrade et al., 2002). Wilson (1955) introduced this procedure and proposed to dissolve the sample with a cold mixture of HF and an acid solution of ammonium metavanadate. This way the Fe(II) is immediately oxidized into Fe(III), and at the same time the vanadate ions (V^{5+}) are reduced to vanadyl (V^{4+}) (1). Then the extra vanadate is determined by titration with $(NH_4)_2Fe(SO_4)_2$ x $6H_2O$, and a solution containing only the reagents. By difference, it is possible to quantify the amount of Fe(II) in the sample. This procedure usually takes around 24 hours, over that time several secondary reactions can occur, such as the oxidation of vanadyl by a reverse reaction with Fe(III), which is rendered unimportant.

$$VO_2^{+} + Fe^{2+} + 2H^{+} \rightarrow VO^{2+} + fe^{3+} + H_2O \qquad (1)$$